Renewable Energy 240 (2025) 122168

Contents lists available at ScienceDirect

Renewable Energy

journal homepage: www.elsevier.com/locate/renene

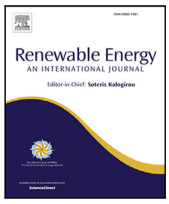

A probabilistic risk assessment framework for the impact assessment of extreme events on renewable power plant components

Nadia N. Sánchez-Pozo [a], Erik Vanem [b,c], Hannah Bloomfield [d,e], Jose I. Aizpurua [f,g,*]

[a] Mondragon University, Loramendi, 4., Mondragón, 20500, Spain
[b] DNV, Veritasveien 1, Hovik, 1363, Norway
[c] University of Oslo, Problemveien 11, Oslo, 0313, Norway
[d] School of Engineering, Newcastle University, Mertz Court, Newcastle upon Tyne, NE1 7RU, United Kingdom
[e] School of Geographical Sciences, University of Bristol, University Road, Bristol, BS8 1SS, United Kingdom
[f] University of the Basque Country (UPV/EHU), Faculty of Informatics, Department of Computer Science & Artificial Intelligence, Manuel de Lardizabal P., 1, Donostia - San Sebastián, 20018, Spain
[g] Ikerbasque, Basque Foundation for Science, Euskadi Plaza, 5, Bilbao, 48009, Spain

ARTICLE INFO

Keywords:
Extreme events
Degradation
Risk
Transformers
PV panels

ABSTRACT

Climate change is expected to worsen the frequency, intensity, and impacts of extreme weather events. Renewable energy sources (RESs) play a key role in the decarbonization process to decelerate climate change effects. However, extreme events pose a significant threat to renewable energy infrastructure. Accordingly, understanding the impacts of extremes on RESs becomes crucial to ensure the reliability of power grids. In this context, this research presents a novel probabilistic risk assessment framework to evaluate the degradation of wind turbine transformers (WTTs) and photovoltaic (PV) panels in the face of extreme weather conditions. The framework uses a Gaussian copula to model the joint probability of extreme events, effectively incorporating multivariate phenomena. Case studies involving WTTs and PV panels operated in different wind and solar power plants, illustrate the effectiveness of the proposed methodology, demonstrating its ability to capture the combined influence of different meteorological variables on degradation rates. These results underscore the potential of this framework to assess weather-related risks in renewable energy systems, thereby enhancing their resilience and reliability.

1. Introduction

Climate change presents a significant threat to the health of the planet and the reliability of renewable energy systems. In recent decades, scientific evidence has clearly demonstrated an alarming trend of rising global temperatures, changing weather patterns, and escalating extreme weather events [1,2]. The increase of extreme events, such as storms, pose a significant threat to the reliability of renewable energy systems, increasing the vulnerability of power components to extreme conditions. The increasing frequency and intensity of extreme weather events, such as hurricanes, floods, and wildfires [3], can cause severe damage to power and energy infrastructure and renewable energy technology in particular, including wind turbines, solar panels, and hydroelectric power plants [4]. These disruptions can significantly impact energy production, causing blackouts and hindering the transition to a sustainable energy future [5].

Energy meteorology is the field of study focused on the analysis of the influence of the weather and climate on energy systems. It is an important field for understanding and mitigating the impacts of extreme weather events on energy infrastructure and ensuring the reliable and efficient delivery of energy [6,7].

Extreme event modeling encompasses a wide range of statistical and mathematical techniques used to analyze and predict the occurrence and severity of rare, high-impact events. These techniques, ranging from traditional statistical methods to advanced machine learning (ML) algorithms, are essential to understand the risks associated with extreme events and inform timely decision-making strategies.

In the context of wind energy systems, Tedesco et al. develop an innovative approach to model weak-wind events using copulas [8]. This approach has significant implications for the design and operation of wind energy systems (WES) and provides a valuable tool for analyzing the behavior of wind patterns under varying atmospheric

* Corresponding author at: University of the Basque Country (UPV/EHU), Faculty of Informatics, Department of Computer Science & Artificial Intelligence, Manuel de Lardizabal P., 1, Donostia - San Sebastián, 20018, Spain.
E-mail addresses: nsanchez@mondragon.edu (N.N. Sánchez-Pozo), joxe.aizpurua@ehu.eus (J.I. Aizpurua).

https://doi.org/10.1016/j.renene.2024.122168
Received 13 May 2024; Received in revised form 4 December 2024; Accepted 12 December 2024
Available online 19 December 2024

Nomenclature

Abbreviations

CM	Copper Mountain
CDF	Cumulative Distribution Function
CNN	Convolutional Neural Networks
DL	Deep learning
EVT	Extreme Value Theory
FM	failure mode
GMMs	Gaussian Mixture Models
HST	Hottest-Spot Temperature
ML	Machine Learning
MLE	Maximum Likelihood Estimation
MS	Mount Signal
n-sMC	non-sequential Monte Carlo
PV	PhotoVoltaic
RUL	Remaining Useful Life
RESs	Renewable Energy Sources
s-MC	sequential Monte Carlo
TOT	Top Oil Temperature
WES	Wind Energy Systems
WTT	Wind Turbine Transformers

Nomenclature

β_0	Frequency factor
β_1	Activation energy
β_2	Effect of cyclic temperature
β_3	UV radiation effect
β_4	RH effect
C	Consequence
Θ^{-1}	Inverse CDF of a standard normal distribution
Θ_A	Ambient temperature [°C]
Θ_R	CDF of a multivariate Gaussian distribution
$C_R^{Gauss}(u)$	Multivariate Gaussian copula
D	Difference operation
$F_{A_{PV}}$	PV aging factor [year^{-1}]
$GPOA$	Solar irradiance in the plane of the PV array [W/m^2]
k	Boltzmann constant
O	Undesired event
$Pr(O)$	Probability of occurrence
R	Covariance matrix
RH_{daily}	Humidity [%]
UV_{daily}	Daily average irradiation [W/m^2]
W_s	Wind speed [m/s]
$\Delta\theta_H(t)$	HST rise, over top-oil temperature at instant t [°C]
$\Delta\Theta_{daily}$	Daily average temperature [K]
$\Delta\theta_{H,R}(t)$	HST rise at rated load, at instant t [°C]
τ_{TO}	oil time constant [mins.]
τ_W	winding time constant [mins.]
$\theta_H(t)$	Hottest spot temperature at instant t [°C]
$\theta_A(t)$	Ambient temperature at instant t [°C]
Θ_{max}	Maximum temperature [K]
Θ_{mod}	Operating temperature of the PV module
$\theta_{TO}(t)$	Top-oil temperature at instant t [°C]
$i(t)$	Load at instant t [A]
$i_r(t)$	Rated load at instant t [A]
k_{11}, k_{21}, k_{22}	thermal constants [-]
K(t)	Normalized load at t [p.u.]
R	Ratio of load losses to no load losses [W]
V(t)	Insulation aging rate at t [hours]
x	oil exponent constant [-]
y	winding exponent constant [-]

conditions [8]. Similarly, Bloomfield et al. developed a flood severity index, which provides a comprehensive measure of flood risk [9]. This index can be used to inform flood preparation and mitigation strategies.

The use of risk matrix methods has been also explored for solar PV, hydropower, biomass, and biogas to assess the vulnerability of these renewable energy sources (RESs) to extreme weather events [10].

Furthermore, in ocean engineering applications, the use of environmental contours offers a valuable tool for designing structures like offshore platforms and ships [11]. Environmental contours map the probability of joint occurrence of critical environmental variables, such as wave height and wind speed, allowing engineers to identify the most likely extreme conditions that a structure might encounter, ensuring its safe and robust design [12].

Deep learning (DL) is a branch of ML which has emerged as a powerful tool with immense potential to revolutionize energy meteorology. Notable advances in this area include probabilistic forecasts of extreme heat waves using convolutional neural networks (CNNs). CNNs have demonstrated the potential to improve the accuracy and reliability of weather forecasts [13]. This can lead to more informed decisions regarding energy production and grid management during extreme heat events. DL has been also applied to develop a risk index for the design of offshore energy infrastructure and it has shown to be a valuable approach for assessing the impact of metocean variables [14]. In the offshore arena, Vanem evaluated the impact of extreme events using extreme value theory (EVT) [15] and serial correlation dependencies [16].

The evaluation of the impact of extreme events on energy systems is a challenging task due to the complex nature of future weather conditions. A stochastic robust optimization method has been introduced to address this issue, taking into account low impact variations and high impact extreme events [17]. A study highlighted in [18] has identified a decline in wind turbine performance with age, leading to reduced efficiency and increased maintenance costs over time. Other researchers, as reported in [19], have explored the effective use of vine copulas in modeling the spatio-temporal dependence of load and wind power. Furthermore, [20] has developed a novel model to predict wind power and anticipate potential grid failures during meteorological disasters.

In the area of wind power uncertainty, [21] proposes an innovative approach based on k-means clustering and Gaussian Mixture Models (GMMs) for operational risk assessment. Furthermore, a recent study presented in [22] introduces a non-sequential Monte Carlo (n-sMC) method to assess the risk of power systems under extreme typhoon events. In particular, this method is shown to be more efficient than traditional sequential Monte Carlo (s-MC) methods. In this direction, studies of wind speed extremes for wind power plants using EVT have provided valuable insights into the distribution of wind speeds at different locations [23]. These findings can inform the design and operation of WES to optimize energy production and minimize damage from extreme wind events. Namely, research on the reliability of extreme wind speeds from EVT has provided valuable insights into the statistical properties of extreme wind events [24]. These findings can be used to improve the accuracy of extreme event forecasts and risk assessments.

Table 1
Recent works on energy meteorology and risk index.

Ref.	Extremes	Methods	Renewables	Aging
[9]	Wind	Copulas	Yes	No
[16]	Wind, Wave	EVT	Yes	No
[20]	Wind	SVM	Yes	No
[17]	PV	SRO	Yes	No
[19]	Wind	Copulas	Yes	No
[25]	Wind	Copulas	Yes	No
[26]	Wind, PV	Copulas	Yes	No
[21]	Wind, PV	GMMs	Yes	Yes
[27]	Wind	GMMs	Yes	No
[22]	Wind,	n-sMC	Yes	Yes
Ours	**Wind, PV**	**Copulas**	Yes	Yes

Table 1 displays the synthesis of related work organized according to types of extreme events, evaluation methods, evaluation of the impact on renewable energy and evaluation of the impact on aging.

It can be seen from Table 1 that there is no approach that simultaneously considers the quantification of the occurrence of extreme events and their impact on the aging of the components of renewable energy [21,22]. As for specific extreme event modeling methodologies, the literature focuses on either the quantification of extreme events or the impact on aging, but not both simultaneously. For example, some approaches use extreme value theory (EVT) to estimate the probability of extreme events, while others use reliability theory to model the degradation of components with age. However, there is a need for a more holistic approach that integrates both types of modeling to fully understand and predict the impact of extreme events on renewable energy systems.

Climate change is reshaping weather patterns on a global scale, sparking apprehensions regarding the heightened occurrence and severity of extreme weather phenomena. Nonetheless, this study opts to employ models predicated on the assumption of climatic stationarity throughout the historical data period.

Consequently, the main contribution of this research is the development of a novel risk index approach to assess the impact of extreme events on the degradation of components of renewable energy.

The approach has been tested on wind energy and solar photovoltaic (PV) energy applications operated in different locations, focused on key components such as wind turbine transformers (WTTs) and PV solar panels.

Key meteorological variables, which are essential for the modeling of WTTs and PV solar panels, are also directly influenced by climate change, such as temperature, radiation, wind speed, and relative humidity. Rising temperatures reduce the efficiency of PV panels, changing radiation levels affect solar energy harvesting, and changing wind patterns affect wind turbine power generation and WTT aging.

The proposed approach enables the quantification of the risk level associated with the potential impact of extreme events on the power system and its constituent components. The extreme aging risk information inferred from the framework is very valuable, and it can be used by the power plant operators to take preventive decisions related to operation and maintenance (O&M) actions of the analyzed power components in the presence of extreme events.

The impact of the proposed approach may vary depending on the region because large-scale weather patterns differ significantly across the globe. The approach has been evaluated in different wind and solar farm locations in Vietnam, United States, and Greece. The proposed risk index approach can be applied to any location, but it requires the adaptation and calibration of models for specific regions with unique weather conditions.

The remainder of this paper is organized as follows. Section 2 describes the proposed methodology. The case studies and obtained results are discussed in detail in Sections 3 and 4, respectively. Finally, Section 5 discusses the obtained results and the proposed approach, and Section 6 concludes.

2. Proposed risk assessment approach

The risk index of any system is defined as the combination of the probability of occurrence of an event combined with the consequence, defined as follows [28]:

$$Risk = Pr(O) \times C \tag{1}$$

where $Pr(O)$ denotes the probability of occurrence of the undesired event, O, and C denotes, the consequence.

In the context of energy meteorology, the adaptation of Eq. (1) into the specific weather-dependent energy system is needed. Consequently, Fig. 1 shows the proposed risk assessment framework focused on components operated in renewable energy power plants.

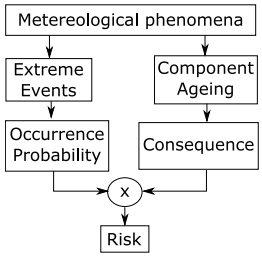

Fig. 1. Risk assessment framework for RES operated assets.

From Fig. 1 it can be observed that the occurrence probability of extreme events and aging of power components are connected through the meteorological phenomena, which causes a risk index variation. The effect of meteorological events on power components is a multifactorial phenomenon, and therefore, the joint occurrence of extreme events should be captured. Accordingly, this research work captures the occurrence probability of extreme events through copulas.

The consequence of the impact of extreme meteorological events is modeled through the aging model of the component under study, which is the direct result of the meteorological dependencies of the component. The aging models are implemented as cumulative aging processes. Each aging cycle has its own strength and, in the case of extreme events, they may have a considerable impact on asset lifetime. Therefore, the outcome of the proposed approach is the combination of extreme event occurrence probability with aging levels, *i.e.* extreme aging risks.

Fig. 2 shows the implementation of the proposed risk assessment approach. The process starts from the key component selection which is prone to suffer from meteorological extreme events. This selection is followed by the failure mode (FM) assessment, which is a representation of the main aging mechanism of the selected component.

After the selection process, there are two main stages: (i) extreme occurrence modeling based on the environmental factors that influence the aging of the component under study and (ii) extreme event risk modeling based on the aging model, which are described in the following sections. Both stages are combined into an extreme risk aging model, which can infer the probability of being an extreme event, given the testing data $p(extreme|data)$.

2.1. Occurrence probability & copulas

Extreme events are generally caused by a set of complex interdependent phenomena, such as wind, pressure and temperature [17,29]. In this context, moving beyond the evaluation of the extreme value of individual variables as in classical EVT [16], copula-based methods have been shown to adequately articulate and model the structure of interdependencies between random variables [25].

Classical sample-based correlation methods, e.g. Pearson or Spearman's rank correlation, do not integrate trends and dependencies. These methods assume that the relationship between the variables is stationary and independent of time or order.

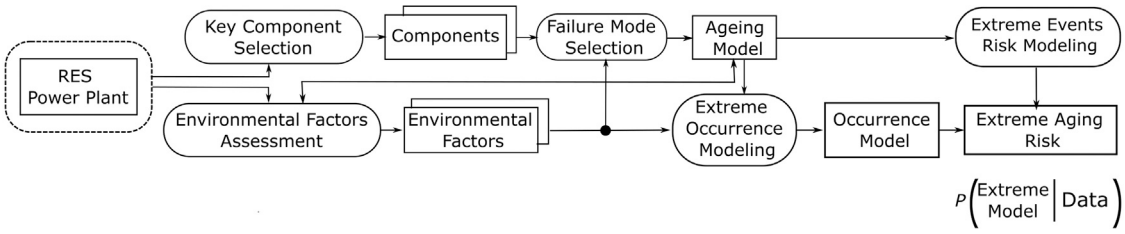

Fig. 2. Extreme event modeling approach for components operated in RES power plants.

Alternatively, copulas can capture complex modeling phenomena through multivariate distributions and dependencies between distributions [30]. Copula-based methods support the construction of detailed multivariate distributions and enhance the ability to capture and manage the complexity associated with extreme events by defining the marginal distributions and the copula independently.

Assuming that the vector of random variables $X = \{X_1, \ldots, X_d\}$, which after the integral transform are converted into a probability vector $u = \{u_1, \ldots, u_d\}$ over $[0,1]^d$, with each $u_i \in [0,1]$, with the cumulative distribution function (CDF), F, defined as $F(\boldsymbol{u}) = Pr(\boldsymbol{U} \leq \boldsymbol{u})$, a copula, C, is defined as the joint CDF with uniform marginals. Formally, it is defined as [30]:

$$C(u_1, \ldots, u_d) = Pr(U_1 \leq u_1, \ldots, U_d \leq u_d) \tag{2}$$

According to Sklar's theorem, any multivariate joint distribution of these random variables can be expressed as a function of their individual marginal distributions, F and the copula C [31]. This relationship allows us to model the marginal behavior and dependence structure separately, potentially simplifying the modeling process for complex multivariate distributions.

Assuming two random variables, X and Y, with their CDFs $u = F_X(x)$ and $v = F_Y(y)$, through the Sklar's theorem the copula density function, $c(u, v)$, is estimated from the derivative of C with respect to each of its arguments:

$$c(u, v) = \frac{f_{XY}(x, y)}{f_X(x) f_Y(y)} \tag{3}$$

where $f_X(x)$ and $f_Y(y)$ are the marginal PDFs of X and Y, respectively.

Importantly, copulas are able to grasp linear and nonlinear dependencies. To this end, they use rank correlations. Rank correlations require monotonic functions and evaluate how well the relationship between two variables can be described using a monotonic function. Since copulas are described with distribution functions, the monotonicity requirement is satisfied.

There exist various copula functions, and their applicability depends on the underlying data structure. Multivariate Gaussian copulas have demonstrated utility in capturing specific types of extreme events, and if the underlying dataset demonstrates the Gaussian dependence structure, e.g. through goodness-of-fit tests, they may be used due to their convenient underlying structure [25], which have the form:

$$\mathbf{C}_{\mathbf{R}}^{\text{Gauss}}(\mathbf{u}) = \boldsymbol{\Phi}_{\mathbf{R}}(\boldsymbol{\Phi}^{-1}(u_1), \ldots, \boldsymbol{\Phi}^{-1}(u_d)) \tag{4}$$

where $\boldsymbol{R} \in [-1, 1]$ is the correlation matrix of the random variables and $\boldsymbol{\Phi}^{-1}$ is the inverse CDF of a standard normal distribution and $\boldsymbol{\Phi}_{\boldsymbol{R}}$ is the CDF of a multivariate Gaussian distribution with mean vector zero and covariance matrix R. Therefore, the copula density function is:

$$C_{\mathbf{R}}^{\text{Gauss}}(\mathbf{u}) = \frac{1}{\sqrt{|\mathbf{R}|}} \exp\left(-\frac{1}{2} \begin{pmatrix} \boldsymbol{\Phi}^{-1}(u_1) \\ \vdots \\ \boldsymbol{\Phi}^{-1}(u_d) \end{pmatrix}^T (R^{-1} - I) \begin{pmatrix} \boldsymbol{\Phi}^{-1}(u_1) \\ \vdots \\ \boldsymbol{\Phi}^{-1}(u_d) \end{pmatrix} \right) \tag{5}$$

It can be observed that a Gaussian copula is a multivariate Gaussian distribution with correlation matrix $\mathbf{R}$ and each margin U_i has the integral probability transform $\boldsymbol{\Phi}^{-1}(u_i)$ applied.

To model a multivariate Gaussian copula, it is necessary to transform the random variables to have uniform marginal distributions within the interval [0, 1] [32]. This transformation can be done using parametric and nonparametric methods. In this study, nonparametric estimation was used, specifically using quantile-based normalization to convert the data into a standard normal distribution. The goodness of fit for the marginal distributions was assessed using the Kolmogorov–Smirnov test, with parameters estimated through maximum likelihood estimation (MLE). Subsequently, MLE was also utilized to estimate the copula parameters. Finally, the copula model was selected based on the Akaike Information Criterion

Fig. 3 shows the occurrence model. The process starts by splitting the training and testing datasets for model design and validation, respectively.

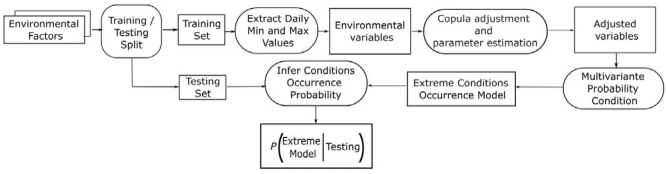

Fig. 3. Occurrence model design and testing approach.

Using the training set to model and learn the occurrence probability of extreme events, hourly sampled time-series are downsampled to daily maximum and minimum values of the analyzed meteorological phenomena. Accordingly, the `environmental variables` signal is obtained across a time period of interest.

Subsequently, to capture the dependencies of meteorological extreme events, first the input data are adjusted to have uniform marginal distributions (`adjusted variables`), and then the joint occurrence probability structure of meteorological variables is learned through copulas (`extreme conditions occurrence model`).

Consequently, when observing new events, the likelihood of being an extreme event can be quantified, according to the learned probabilistic model.

In this case, the tails of the distribution of meteorological phenomena are analyzed, establishing a threshold based on standard deviations. An event is considered extreme if its value falls within ±2 standard deviations from the mean. The Cumulative Distribution Function (CDF) is calculated to quantify the cumulative occurrence probability of an extreme event, which provides the probability that a random variable takes on a value less than or equal to a specific threshold. Fig. 9 illustrates extreme events marked in red over a 10-year period. These events correspond to observed data points, which result in cumulative occurrence probability values above 0.8.

The built model is tested with the test set, which includes unseen meteorological data for testing and validation purposes.

The sensitivity of the considered (i) timescale, e.g., daily, weekly, or monthly data, and (ii) extreme value condition, e.g., maximum value, 95th percentile and 75th percentile, may affect the learned occurrence probability model. The selection of different percentiles aims to encompass a range of severity levels. Reference is made to Section 5 for an extended discussion on the area.

2.2. Consequence & degradation

The consequence of an extreme event is specific to the component under study. This research focuses on WTTs and PV panels. In order to evaluate the impact of the extreme events, analytic lifetime models for transformers and PV panels are used, which directly depend on the analyzed meteorological phenomena.

There are different failure modes that can cause the degradation of WTTs and PV panels and the effect of different failure modes on the degradation of components is different. Some failure modes do not result in immediate losses in efficiency. Instead, they lead to a gradual decline in module performance. A critical latent failure mode of WTTs is partial discharge (PD), which progressively degrades the insulation system. While PD may not immediately impair transformer performance, its cumulative effect can result in insulation breakdown and eventual system failure if unaddressed [33]. As for PV panels, microcracking or delamination can lead to lifetime and reliability reduction without an impact on electrical performance [34,35]. Accordingly, the main failure modes analyzed in this study for WTT and PV panels have been focused on thermal degradation events and their impact on lifetime reduction, without direct consideration of their effect on electrical performance.

Wind Turbine Transformers (WTT)

The health of WTT is defined in agreement with Eq. (16) and the main stress factor is the hottest-spot temperature (HST). In turn, the HST is estimated from indirect variables [cf. Eq. (7)]. Accordingly, the main meteorological events that affect the health of WTTs are a bivariate problem. The hourly ambient 2-meter temperature is directly obtained from the ERA5 reanalysis data set [36].

Extreme meteorological events that affect the health of WTTs are ambient temperature and wind speed. Ambient temperature directly impacts aging [cf. Eq. (16)] and wind speed affects aging through wind-to-power conversion of the wind turbine and associated load flowing through the transformer.

The power generated by the wind turbine will flow through the transformer, and depending on the generated load, the HST of the transformer insulation will increase. Therefore, the wind speed plays an important role in power generation and transformer aging. Accordingly, using the ERA5 reanalysis dataset, the hourly wind speed, ws, is calculated from the component vector winds, u and v, at 100 m wind speeds as follows [36]:

$$ws = \sqrt{u^2 + v^2} \tag{6}$$

where u is the eastward component of the wind and v is the northward component of the wind, both in m/s.

The wind farms analyzed use different types of wind turbines. Namely, the US wind farm uses Mitsubishi MWT-1000-61 turbines (1 MW, rotor diameter 61.4 m), Vietnam's wind farm uses Siemens-Gamesa SG 3.4-132 turbines (3.4 MW, rotor diameter 132 meters), and finally Greece uses Nordex N100/3300 (3.3 MW, diameter 100 m) wind turbines. If a direct mapping of the turbine was not available in the `windpowerlib` library, without loss of generality, an equivalent turbine was used (MWT-1000, SG 3.4) [37].

2.2.1. Transformer degradation modeling

Transformers are critical elements in power and energy systems in general and in RESs in particular [38]. Focusing on WES, they convert the variable voltage produced by the generator to a stable voltage for transmission to the grid [39].

The performance and lifetime of transformers are affected by several factors, including operational stress, environmental conditions, and maintenance practices. Among these factors, meteorological variables play a key role in transformer degradation. Namely, ambient temperature and wind speed can significantly affect the thermal and mechanical properties of transformer materials, resulting in accelerated degradation [39].

Thermal modeling

The HST is the temperature that most affects aging. However, HST measurements are challenging and expensive, and, generally, they are estimated from indirect measurements:

$$\Theta_{\mathbf{H}}(t) = \Theta_{\mathbf{TO}}(t) + \Delta\Theta_{\mathbf{H}}(t) \tag{7}$$

where $\Delta\Theta_{\mathbf{H}}(t)$ is the HST rise over top-oil temperature (TOT) and $\Theta_{\mathbf{TO}}(t)$ is the TOT defined as follows:

$$\Delta\Theta_{\mathbf{TO,R}}\left(\frac{1+K(t)^2R}{1+R}\right)^x = k_{11}\tau_{\mathbf{TO}}\frac{d\Theta_{\mathbf{TO}}(t)}{dt} + \Theta_{\mathbf{TO}}(t) - \Theta_{\mathbf{A}}(t) \tag{8}$$

where $K(t) = \frac{I(t)}{I_r}$, $I(t)$ is the load at instant t and I_r the rated load, R is the ratio of load losses to non-load losses, x is the oil exponent constant, which models the exponential power of total losses with respect to TOT heating, τ_{TO} is the oil time constant, $\Delta\Theta_{TO,R}$ is the TOT rise at rated load, k_{11} is a thermal constant determined through experimentation and $\Theta_A(t)$ is the ambient temperature.

The HST rise, $\Delta\Theta_H(t)$, is calculated as:

$$\Delta\Theta_H(t) = \Delta\Theta_{H_1}(t) - \Delta\Theta_{H_2}(t) \tag{9}$$

where $\Delta\Theta_{H_1}(t)$ models the oil heating without HST variations:

$$k_{21}\Delta\Theta_{H,R}K(t)^y = k_{22}\tau_w\frac{d\Theta_{H_1}(t)}{dt} + \Delta\Theta_{H_1}(t) \tag{10}$$

$\Delta\Theta_{H_2}(t)$ models the HST variations:

$$(k_{21}-1)\Delta\Theta_{H,R}K(t)^y = (\tau_{TO}/k_{22})\frac{d\Theta_{H_2}(t)}{dt} + \Delta\Theta_{H_2}(t) \tag{11}$$

where τ_w is the winding time constant, $\Delta\Theta_{H,R}$ is the HST rise at rated load, y is the winding exponent constant, which models the loading exponential power with the heating of the windings, k_{21} and k_{22} are the transformer thermal constants. The following design parameters have been used [40]: τ_{TO} = 180 [min]; τ_w = 4 [min], ; k_{11} = 0.75; k_{21} = 2.32; k_{22} = 2.05; $\Delta\Theta_{TO,R}$ = 54.26 °C; $\Delta\Theta_{H,R}$ = 15.1 °C.

Assuming d/dt is a small-time difference, differential equations are turned into difference equations and the TOT in Eq. (8) is calculated as follows [40]:

$$\begin{aligned}\Theta_{TO}(t) &= D\Theta_{TO}(t) + \Theta_{TO}(t-1)\\ D\Theta_{TO}(t) &= \frac{\Delta t}{k_{11}\tau_{TO}}\left[\Delta\Theta_{TO,R}\left(\frac{1+K(t)^2R}{1+R}\right)^x + \Theta_A(t) - \Theta_{TO}(t)\right]\end{aligned} \tag{12}$$

where D denotes a difference operation of the associated variable within the period Δt. Similarly, Eqs. (10) and (11) can be rewritten as follows:

$$\Delta\Theta_{H_i}(t) = D\Delta\Theta_{H_i}(t) + \Delta\Theta_{H_i}(t-1) \tag{13}$$

for i={1,2}, where

$$\begin{aligned}D\Delta\Theta_{H_1}(t) &= \frac{\Delta t}{k_{22}\tau_w}\left[k_{21}\Delta\Theta_{H,R}K(t)^y - \Delta\Theta_{H_1}(t)\right]\\ D\Delta\Theta_{H_2}(t) &= \frac{k_{22}\Delta t}{\tau_{TO}}\left[(k_{21}-1)\Delta\Theta_{H,R}K(t)^y - \Delta\Theta_{H_2}(t)\right]\end{aligned} \tag{14}$$

Finally, assuming steady-state initial conditions, the initial conditions are defined as follows:

$$\begin{aligned}\Theta_H(0) &= \Theta_{TO}(0) + k_{21}\Delta\Theta_{H,R}K(0)^y - (k_{21}-1)\Delta\Theta_{H,R}K(0)^y\\ \Theta_{TO}(0) &= \Theta_A(0) + \Delta\Theta_{TO,R}\left(\frac{1+K(0)^2R}{1+R}\right)^x\end{aligned} \tag{15}$$

To guarantee numerical stability, Δt should be as small as possible, and never greater than half of the smaller time constant.

Lifetime model

The IEC 60076-7 standard defines insulation paper aging acceleration factor at time t, $v(t)$, as [40]:

$$v(t) = 2^{(98-\Theta_H(t))/6} \tag{16}$$

The aging acceleration factor, $v(t)$, models the instantaneous loss-of-life of the insulation of the transformer. The insulation loss of life over a period, T, *i.e.*, $LOL_{Tr}(T)$, with a timestep, Δt, can be calculated from the cumulative sum of the aging acceleration factor [40]:

$$LoL_{Tr}(T) = \sum_{i=1}^{T} v(t_i)\Delta t \tag{17}$$

Note that the loss-of-life is sequentially calculated to estimate the latest aging state. Note that the IEC assumes an expected life of 30 years, with a reference HST of 98 °C for non-thermally upgraded insulation paper [40]. HST temperature values above this threshold value cause severe damage to the transformer insulation [39].

PV panels

The aging factor of PV panels is defined by Eq. (19). It can be observed that the main aging factor is the thermal stress. In turn, the aging factor is directly dependent on different meteorological phenomena including ambient temperature, solar irradiation, and relative humidity, *i.e.* it is a 3-dimensional problem. Note that wind speed has been considered for degradation calculations, but it has not been included in the copula models in order to focus in the main influencing factors. Hourly sampled variables are obtained from the National Solar Radiation Data Base (NSRDB) [41].

2.2.2. PV panel degradation modeling

The PV panel is a semiconductor device that converts sunlight into electricity through the PV effect. PV panels are critical elements for PV power generation. In this context, the thermal aging influence on PV lifetime is mainly determined by the surrounding operational conditions.

Thermal modeling

The operating temperature of the PV module can be estimated from the SANDIA temperature model [42]:

$$\Theta_{mod} = \Theta_A + GPOA e^{a+bW_s} \tag{18}$$

where a and b are empirical coefficients (in this work, $a = -3.47$ and $b = -0.0594$, according to [42]), W_s is the wind speed [m/s], and Θ_A is the ambient temperature [°C], $GPOA$ is the solar irradiance in the plane of the PV array [W/m^2].

Lifetime model

Kaaya et al., compared different methods for predicting degradation [43], including the Kaaya [44] model and the Sumbramaniyan model [45], both of which were calibrate using data collected from three different sites. However, the two methods produced conflicting results and in certain instances presented inconsistent severity levels for degradation scores. Despite these inconsistencies, both are presented in the IEA report [46] as methods for predicting module degradation based on site-specific environmental variables.

Accordingly, the effect of cyclic temperature on solder bond degradation can be modeled through the PV aging factor, $F_{A_{PV}}$ [year^{-1}], which is defined as follows [47]:

$$F_{A_{PV}}(T, \Delta T, UV, RH) = \beta_0 e^{\frac{-\beta_1}{k_B \Theta_{max}}} \Delta\Theta_{daily}^{\beta_2} UV_{daily}^{\beta_3} RH_{daily}^{\beta_4} \tag{19}$$

where Θ_{max} is the daily maximum temperature of the PV module [K], $\Delta\Theta_{daily}$ is the daily average temperature of the module [K], UV_{daily} is the daily average irradiation [W/m^2], RH_{daily} is the daily average relative humidity [%] and k is the Boltzmann constant. The rest of coefficients, are defined as follows [47]: β_0, frequency factor (0.28), β_1, activation energy, (0.72), β_2, effect of cyclic temperature, (2.63), β_3, UV radiation effect (0.95), and, β_4, RH effect (1.60). Refer to Appendix A for a detailed analysis of different factors on PV aging.

The aging acceleration factor, $F_{A_{PV}}$, models the instantaneous loss of life of the PV panel. The panel loss of life over a period, T, *i.e.*, $LOL_{PV}(T)$, with a timestep, Δt, can be calculated from the cumulative sum of the aging acceleration factor:

$$LoL_{PV}(T) = \sum_{i=1}^{T} F_{A_{PV}}(T_i, \Delta T, UV, RH)\Delta t \tag{20}$$

Software and tools

The proposed risk assessment framework was developed using Python 3.11, with the aid of a range of specialized libraries to facilitate data manipulation, statistical modeling, and visualization. A principal instrument utilized in the analytical process was `Windpowerlib`, a library specifically designed for modeling wind energy systems [37]. To capture the interdependencies between meteorological variables, the `Copulas` library was employed [48]. In particular, the Gaussian multivariate copula model was utilized to capture the relationships between critical environmental factors, including temperature, wind speed, and radiation. For statistical analysis, `SciPy` and `scikit-learn` were utilized to fit distributions to the data and perform kernel density estimation, respectively [49,50]. Finally, `Matplotlib` was employed for the visualization of the results [51].

3. Case studies

The probabilistic occurrence models are based on historical data to adjust parameters (cf. Fig. 3). Accordingly, a strategic split of training–testing data was done to adjust parameters (training), and test models on unseen data (testing). Available datasets cover the 1979–2020 period for wind turbine transformers and 1999–2020 for solar panels. In this respect, copula training was performed with data covering the period 1979–2010 and 1999–2010 for wind and solar energy, respectively. After fitting the copulas with daily maximum values of correlated meteorological values, the performance of the copulas was validated using data from the 2011–2020 period, ensuring that the models were tested on an independent dataset to assess their predictive capability under out-of-sample conditions.

As for the assessed renewable energy power plants, geographically dispersed wind and solar power plants were considered as shown in Fig. 4.

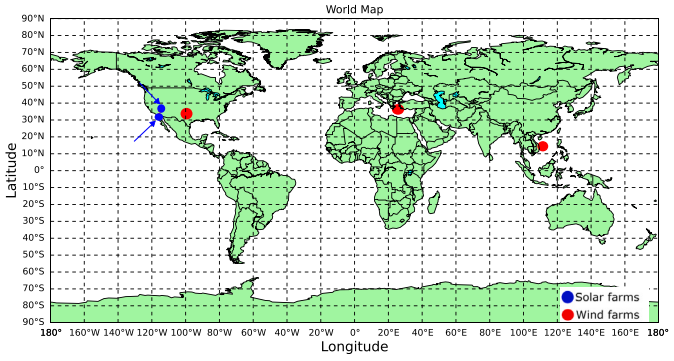

Fig. 4. Location of the considered wind and solar farms.

3.1. Wind energy

Three different geographical locations for wind energy projects were evaluated, including (i) Brazos wind farm in the USA, consisting of 160 wind turbines, 1 MW each; (ii) Phuong Mai in Vietnam, with 6 wind turbines, 20790 W, and finally (iii) Spelia in Greece, 30 MW. Fig. 4 shows the geographic location of the analyzed wind farms.

The areas under study have witnessed various extreme events throughout history. The climate conditions significantly vary in each region, making them susceptible to distinct challenges. These events are anticipated to become more frequent and intense due to climate

change, exacerbating the vulnerability of these areas to climate-related incidents.

Fig. 5 shows the values of wind speed and ambient temperature for summer (June, July, August) and winter months (December, January, February). It can be observed that extreme weather temperature values increase during the summer periods in the locations considered. As for specific locations, it can be observed that during summer extreme events are in the USA characterized by exceptionally high temperatures with an average of 34 °C. In addition, it has the highest average wind speed during the summer, averaging 8.80 m/s. On the contrary, in winter, extreme wind speed events are located in Greece. Note that temperatures are also high in Greece and, at the same time, the associated wind speed. On the contrary, Vietnam experiences the highest average ambient temperature during winter, with an average of 25 °C, surpassing the average of the United States of 15 °C.

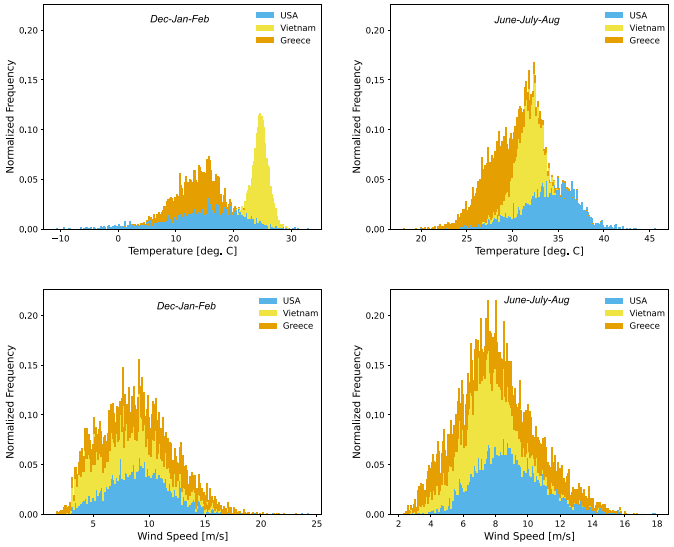

Fig. 5. Climatic conditions for the analyzed wind energy plants during winter and summer seasons (1979–2020).

3.2. Solar energy

Different geographical locations for solar energy projects were evaluated, including the Copper Mountain solar farm, 250 MW, located in Nevada (USA) and Mount Signal Solar II, 154 MW, located in Calexico, California (USA). In this case, geographically close plants were selected to examine similarity in the risk index. Fig. 4 shows their specific location.

Fig. 6 shows the climatic conditions of the considered locations for winter and summer months. Although located in neighboring states, California's Mount Signal (MS) and Nevada's Copper Mountain (CM) exhibit distinct climatic variations. MS experiencing warmer and drier summers and CM experiencing colder and wetter winters. MS experiences the highest average ambient temperature during the summer, with an average of 33 °C. MS receives the highest average solar radiation during the summer, with an average of 567 W/m^2. On the other hand, CM experiences the highest average relative humidity during winter, with an average of 84%, compared to the average of MS of 48%. Additionally, CM has a lower average temperature of −8 °C compared to the average of MS of 14 °C.

4. Numerical results

4.1. Wind Turbine Transformers

Occurrence probability

Accordingly, using the training dataset, firstly their daily maximum values are extracted. Subsequently, after data preprocessing and adjustment, the Gaussian copula is fitted, which will model the occurrence

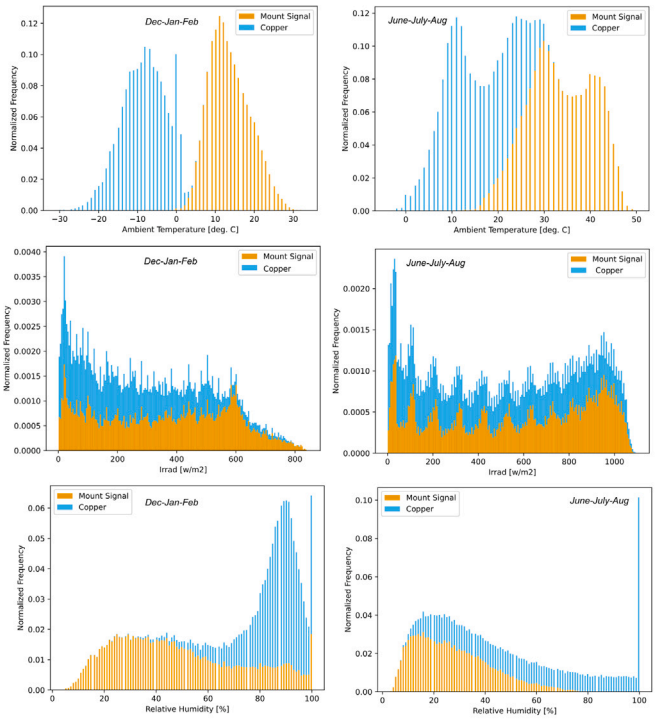

Fig. 6. Climatic conditions for the analyzed solar energy plants during winter and summer seasons (1999–2020).

probability of extreme values which directly impact the WTT aging (cf. Section 2.1). Fig. 7 shows the empirical distributions for USA, Greece and Vietnam using the training set.

The fitted copulas for each location show a high density in specific regions of the temperature-wind speed space. For USA, the highest density is found around 35 °C and 8 m/s. Greece exhibits two regions of high density: 28 °C and 8 m/s, and 15 °C and 8 m/s. Vietnam's copula has its highest density located at 32.5 °C and 7.5 m/s.

The high density regions indicate the most likely joint occurrence of extreme values of ambient temperature and wind speed, in the respective datasets. In this case, daily maximum values have been used to capture extremes (see Section 5 for an extended discussion).

After fitting the copula models, they can be used with unseen test data to evaluate the likelihood of observed hourly samples. Namely, a high probability value would indicate a likely extreme event observed in the training set and vice versa. Consequently, this likelihood can be used to inform the risk index about the probability of the occurrence of extreme meteorological phenomena related to the aging of transformers.

One way to validate the estimated occurrence of an extreme event is to quantify the associated transformer degradation and compare the trends with the maximum and minimum values. That is, extreme events should have the greatest impact on aging and should have associated a high probability of occurrence (cf. Fig. 10).

The K-Sample Anderson–Darling (AD) test was performed to assess the goodness-of-fit of the Gaussian copula model. This test determines if multiple samples come from the same population without assuming a specific distribution. It compares the empirical and theoretical cumulative distribution functions (CDFs), or equivalently, the empirical and estimated copulas. Its critical values are the threshold value corresponding to a chosen significance level (p-value) and the statistical value, which depend on the sample size and the distribution being tested. If the p-value is lower than the critical value (0.05), it indicates a stronger rejection of the null hypothesis that the two copulas are identical. The statistical value measures the discrepancy between the

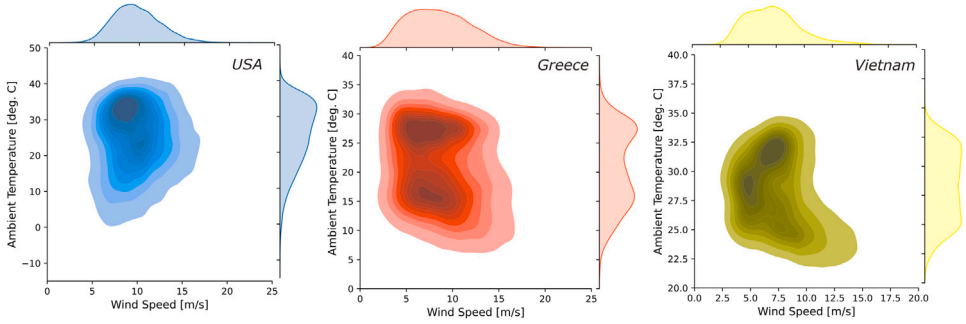

Fig. 7. Empirical distribution for USA, Greece and Vietnam.

empirical and theoretical copulas, with lower values indicating a better fit [52]. The results of the AD tests for the USA, Vietnam, and Greece show consistently high p-values, indicating no significant differences between the observed and fitted distributions. The resulting statistics are as follows. For USA: statistic = −0.1254 and p-value = 0.3250, for Vietnam: statistic = −0.8738, p-value = 0.3250; and for Greece: statistic = 0.1032, p-value = 0.3250. The high p-values > 0.05 indicating no significant difference between the observed and fitted distributions. These results suggest that the model fits the data accurately in each case.

Consequence

The aging of wind turbine transformers is calculated using aging equations that do not have a direct probabilistic interpretation. The aging models determine the impact of observed extreme events on component degradation. However, the relationship between aging events and extreme events comes from the Gaussian copula, which captures the dependency between key meteorological variables during extreme events.

Using the transformer analytic aging model (cf. Section 2.2.1), it is possible to define the instantaneous loss of life of the transformer and its cumulative loss of life (cf. Fig. 8).

To this end, it is necessary to convert the wind speed into a load that flows through the transformer. Accordingly, using the available wind speed data and assuming a specific type of wind turbine, it is possible to estimate the power generated by each turbine. To this end, the `windpowerlib` library has been used, which includes an extensive library of wind turbines [37]. Finally, assuming that the wind turbine transformer has been designed with a ratio of 1:1, the normalized output power can be directly estimated.

Subsequently, using wind speed and ambient temperature time-series corresponding to the test period, the instantaneous transformer aging is calculated using Eq. (16) for different locations. Fig. 8 top shows the hourly aging of the transformer for the wind farms analyzed in different locations, *i.e.* hourly loss of design life of the transformer [cf. Eq. (16)]. The data indicates that transformer aging is a widespread problem, with significant peaks observed in the study locations. It can be seen that the USA suffers the most severe aging conditions, followed by Greece and Vietnam.

Fig. 8-top highlights peak values for each wind farm. Namely, (A) Greece experienced its highest transformer aging peak on August 21, 2010 [53], with a degradation value of 2.88 h of useful life per hour; (B) USA had its peak transformer aging on June 20, 2011 [54], with a degradation value of 8.28 h of useful life per hour; and (C) Vietnam's transformer aging peak occurred on June 12, 2018 [55], with a degradation value of 2.07 h of useful life per hour. The highest peak in Greece suggests that transformers in this region are susceptible to degradation. The peak degradation value in the USA is more than double that of Greece, indicating a more severe aging problem. In contrast, Vietnam's peak degradation value is lower than that of both Greece and the USA, indicating a better overall transformer aging performance in this location.

The integration of instantaneous aging in Fig. 8 over the analyzed operation period, allows the estimation of the cumulative loss of life of the transformer [cf. Eq. (17)]. The USA suffers the most severe transformer aging, amounting to 8219 h of life loss, followed by Greece and Vietnam respectively with 7565 and 3539 h of life loss. When these values are compared to the design life of 180,000 h for WTT [39], the United States exhibits the most severe aging, with a loss of life exceeding 5% of its intended lifespan. Greece's aging pattern is similar, with a loss-of-life of approximately 4.2%. Vietnam, on the other hand, experiences the least aging, with a loss-of-life of approximately 1.97%. These results indicate that considering the insulation aging process, there is room to extend the lifetime of transformers panels.

Fig. 8-bottom shows the cumulative probability distribution (CDF) of the test data (observations). The CDF of the copula represents the cumulative likelihood of the fitted copula values. In this case, copulas are fitted with joint maximum daily values, and therefore, the copula CDF highlights potential extreme events. Namely, Fig. 9 depicts the joint CDF of observed meteorological variables (test data), where extreme values (shown in red) are overlaid based on the established threshold. These values are equivalent to a CDF > 0.8, in Fig. 8-bottom.

Risk

The WTT risk index captures the combined effect of extreme weather event probabilities and WTT aging, assessed using the fitted model and test data. Fig. 10 shows: (1) the maximum cumulative probability of extreme events per year, across all wind farms, and (2) the resulting risk index, indicating the probabilistic risk of extreme weather-induced aging *i.e.* likelihood of accelerated aging due to extreme events.

To analyze the peaks of extreme aging risk, instead of analyzing the resulting risk values in an hourly time-basis, a resampling of the weekly maximum risk values was performed. This process allowed us to identify the maximum weekly aging rate. Accordingly, an analysis of extreme aging risk values and weather variables is presented below. This analysis reveals a clear association between these values and the occurrence probability of extreme weather events.

In particular, the USA wind farm has higher transformer aging risk values than the other wind farms, the extreme risk values peaked at 8.28 h of accelerated aging within a single hour on June 20. This suggests an exceptionally high rate of aging.

At the same time, the ambient temperature rose to 41 °C, accompanied by a brisk wind speed of 14.75 m/s. June 2011 proved to be a month of extreme events, marked by a relentless heat wave and severe drought. The state of Texas experienced temperatures that reached a 43.9 °C [54].

In 2010 and 2012, Greece experienced several extreme weather events, which is typical of the country due to its Mediterranean climate [56]. In 2012, there was an increase in extreme weather events across Greece, according to data from various meteorological stations. Fig. 10 shows that the highest risk of transformer aging in Greece occurred on 21 August 2010, with a value of 2.88 h. On that day, the ambient temperature reached 28 [°C] and the wind speed was 9.82

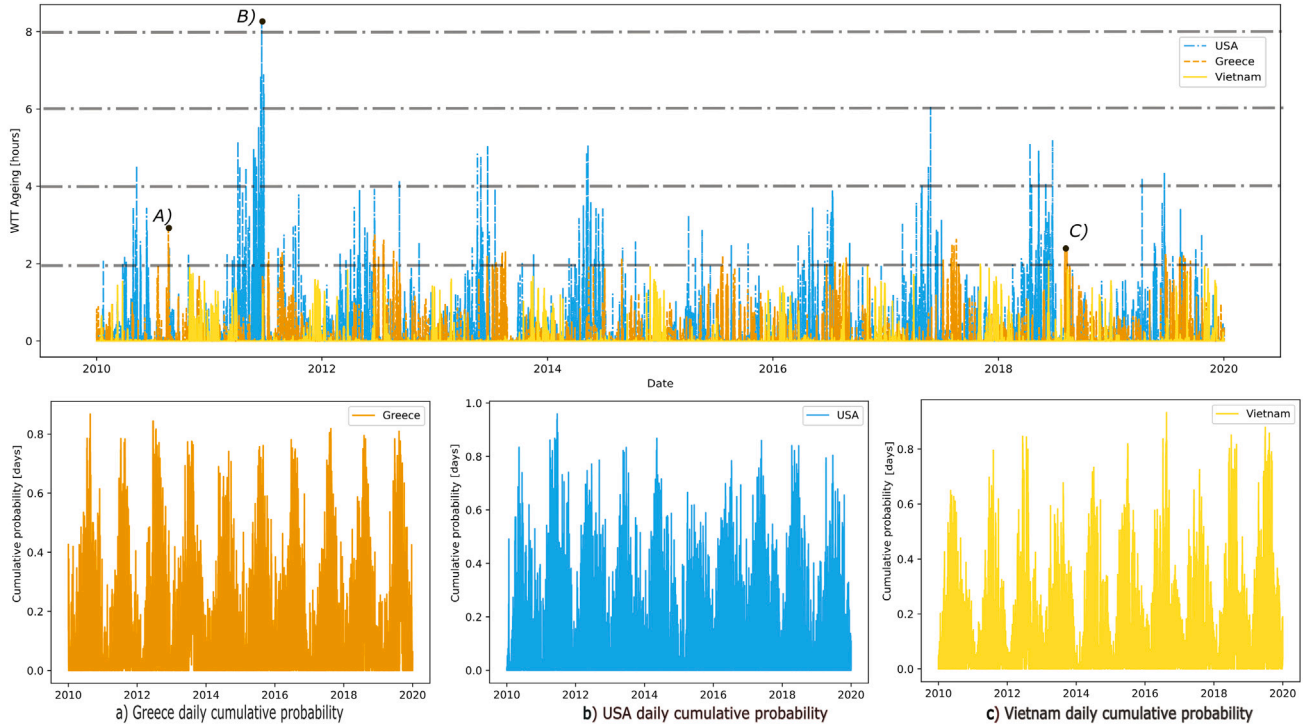

Fig. 8. Instantaneous hourly transformer aging (top). Daily cumulative probability for WTTs in (a) Greece, (b) USA, and (C) Vietnam (bottom).

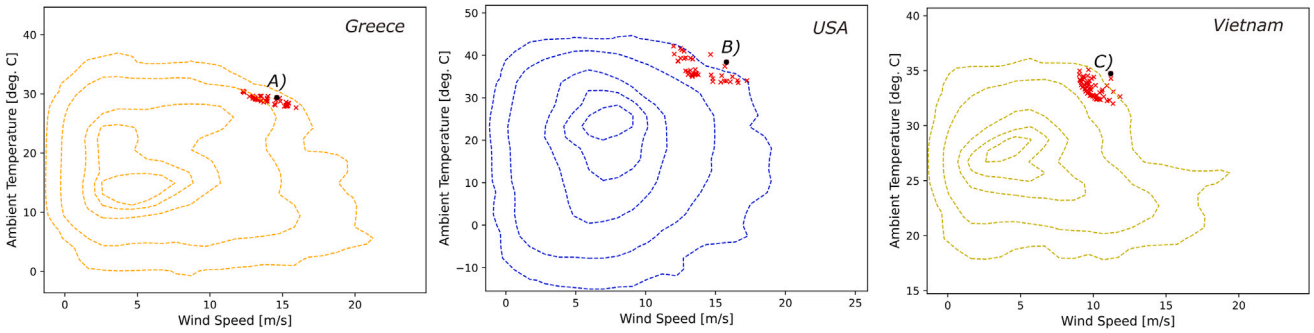

Fig. 9. Joint cumulative probability distribution hourly for WTTs in (a) Greece, (b) USA, and (C) Vietnam.

[m/s]. The second risk peak was observed in 2012, with a value of 2.4 h.

On the other hand, Fig. 10 shows that Vietnam faced the highest risk of transformer aging in both 2016 and 2018. In 2016, the maximum risk was recorded on August 17, reaching a value of 1.76 h. Another significant peak was observed in June 2018. In both years, Vietnam experienced a series of extreme weather events [57]. The combination of high temperatures and dry conditions is believed to have affected WTT, increasing the risk of degradation.

Classification and analysis

Risk was categorized based on the 25th, 75th, and 90th percentiles. Risk event values below the 25th percentile were classified as low risk events, between the 25th and 75th percentiles as moderate risk events, between the 75th and 90th percentiles as high-risk events, and finally, above the 90th percentile as critical risk events. Taking the daily risk values shown in Fig. 10, Table 2 shows the risk levels, along with the corresponding minimum and maximum values for each level, for Vietnam, USA, and Greece. The risk levels are computed from hourly risk values for each day through the testing period.

It can be observed that the distribution of days across the various risk levels is consistent across all three regions, with moderate risk being the most prevalent category. In Vietnam, the highest values for each risk level are relatively low, with the maximum for critical risk reaching 1.76, which is lower than the critical risk values observed in both the USA and Greece. The United States exhibits markedly elevated maximum risk values, particularly within the critical risk category, where the maximum reaches 7.89, exceeding both Vietnam's

Table 2
Risk level classification for wind farms [days].

Farm	Risk level	Min	Max	Count
Vietnam	Low	3.40×10^{-9}	0.000030	914
	Moderate	3.01×10^{-5}	0.002977	1826
	High	2.98×10^{-3}	0.023846	547
	Critical	2.38×10^{-2}	1.764301	366
USA	Low	6.21×10^{-13}	0.000098	914
	Moderate	9.93×10^{-5}	0.096065	1826
	High	9.62×10^{-2}	0.597308	547
	Critical	6.00×10^{-1}	7.898083	366
Greece	Low	2.30×10^{-10}	0.000015	914
	Moderate	1.50×10^{-5}	0.029891	1826
	High	3.01×10^{-2}	0.307067	547
	Critical	3.08×10^{-1}	2.476717	366

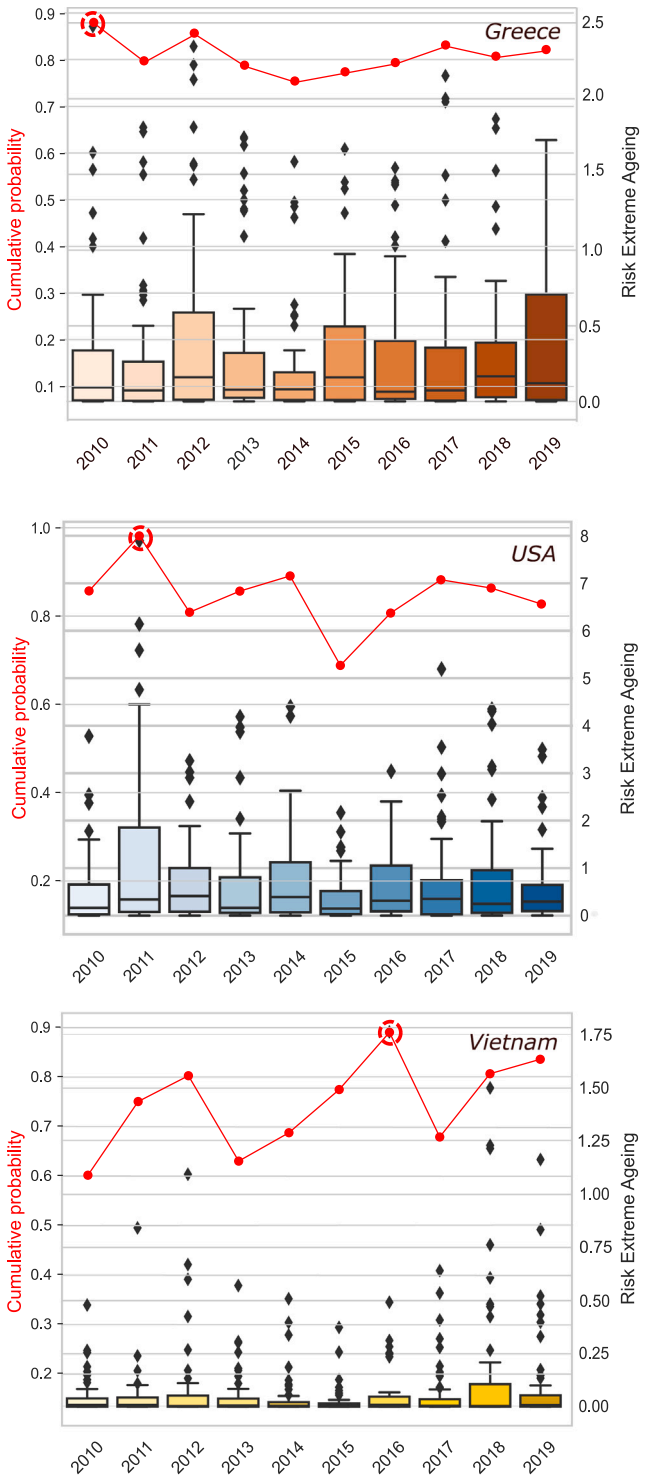

Fig. 10. Extreme event cumulative probability and WTT risk index for different locations.

and Greece's highest values by a considerable margin. The distribution in Greece is somewhat similar to that observed in Vietnam, with critical risk values reaching a maximum of 2.47. While Vietnam exhibits greater uniformity in its risk levels, the USA shows greater variability, indicating a wider range of risk intensities across its period of observation. This comparison suggests that, while all three regions experience comparable distributions of risk across the levels, the USA is exposed to more extreme risk conditions, particularly in the critical risk range.

4.2. Solar energy: PV panels

Occurrence probability

Extreme meteorological events that affect the health of PV panels are solar irradiation, ambient temperature, relative humidity and wind speed [cf. Eq. (19)]. Without loss of generality and in order to focus on the main influencing factors, wind speed has not been considered in the copula models.

Subsequently, the Gaussian copula is fitted to capture the cumulative probability of extreme values, which directly impact the aging of the PV panel. Fig. 11 shows that the Gaussian copula gives results close to the simulated data from the covariance matrix of test data for the PV panels, although there are fewer extreme performances than in the simulated data, and some of the more extreme results have been missed, as observed in the copula for the relative humidity variable.

The goodness-of-fit of the Gaussian copula model was also evaluated using the AD test. For Copper Mountain, the Anderson–Darling test returned a statistic of 6.7879 with a p-value of 0.3250, indicating that we cannot reject the null hypothesis that there is no significant difference between the observed data and the expected distribution. For Mount Signal, the Anderson–Darling test yielded a statistic of 2.7389 with a p-value of 0.3250, similar to Copper Mountain, obtained results indicate no significant difference between the observed and expected distributions.

Consequence

Using the analytic aging model of PV panels (cf. Section 2.2.2), it is possible to define the instantaneous loss-of-life of the PV panels in different locations, as shown in Fig. 12-top.

Fig. 12-top highlights the peak aging values for each location. Namely, (A) Copper Mountain Solar Farm experienced an instantaneous aging peak of 4.15 h on July 23, 2013; and (B) Mount Signal Solar II exhibited a peak instantaneous aging value of 7.52 h on July 31, 2010. The Mount Signal Solar Farm's aging peak is nearly double that of the Copper Mountain Solar Farm, suggesting a more severe aging at this site.

Instantaneous aging was integrated over the testing set of 10 years to estimate the total life loss over the period of operation [cf. Eq. (20)]. The results indicate that aging is more severe at Mount Signal (6628 h), followed by Cooper Mountain (2339 h). The effective lifetime loss relative to the lifetime of the photovoltaic panel (180,000 h) is 3.95% at Mount Signal and 1.4% at Cooper Mountain. These results indicate that there is room to extend the lifetime of PV panels.

Fig. 12-bottom shows the combined cumulative occurrence probability for the observed meteorological variables in the test data. This CDF is conditioned on the copulas shown in Fig. 11, which are fitted from daily maximum values of ambient temperature, relative humidity, and irradiation over the training data.

Fig. 13 shows the joint cumulative probability distribution functions plotted in bivariate plots. This visualization highlights the extreme values (A and B) identified by the CDF thresholds, which are highlighted in red based on a predefined criterion defined in Section 2.1.

Risk

The PV panel risk index combines meteorological extreme event cumulative probabilities and PV panel aging, evaluated for the testing data set period (empirical). In agreement with WTT risk assessment (cf. Fig. 10), a resampling of the weekly maximum risk values was performed to study extreme aging risk peaks.

Accordingly, Fig. 14 shows the cumulative probability of extreme events for each solar farm. Additionally, it presents the obtained risk index, which serves as an indicator of the probabilistic risk of accelerated aging caused by meteorological events. Specifically, this reflects the likelihood of extreme events triggering immediate and significant degradation in the solar farm's components.

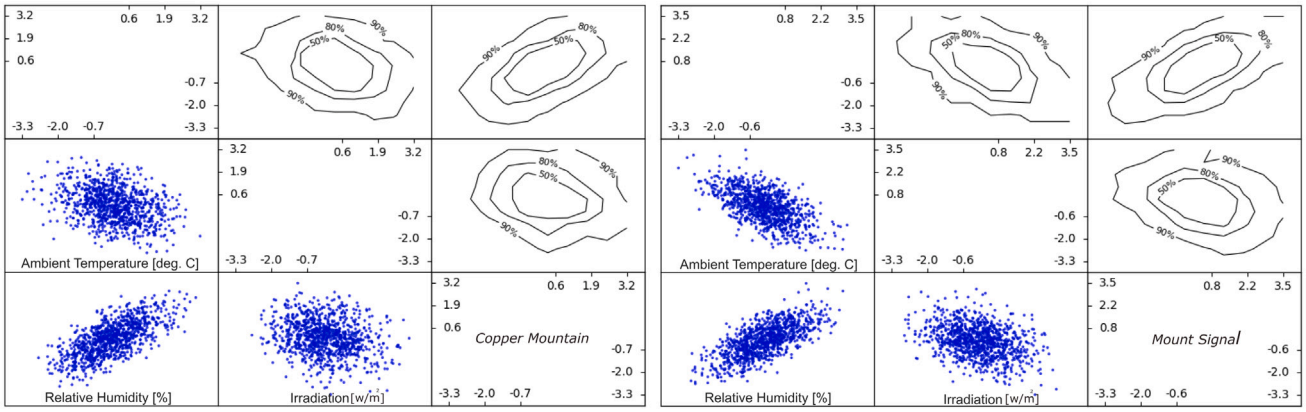

Fig. 11. Simulated cumulative distribution with normalized variables for Copper Mountain and Mount Signal.

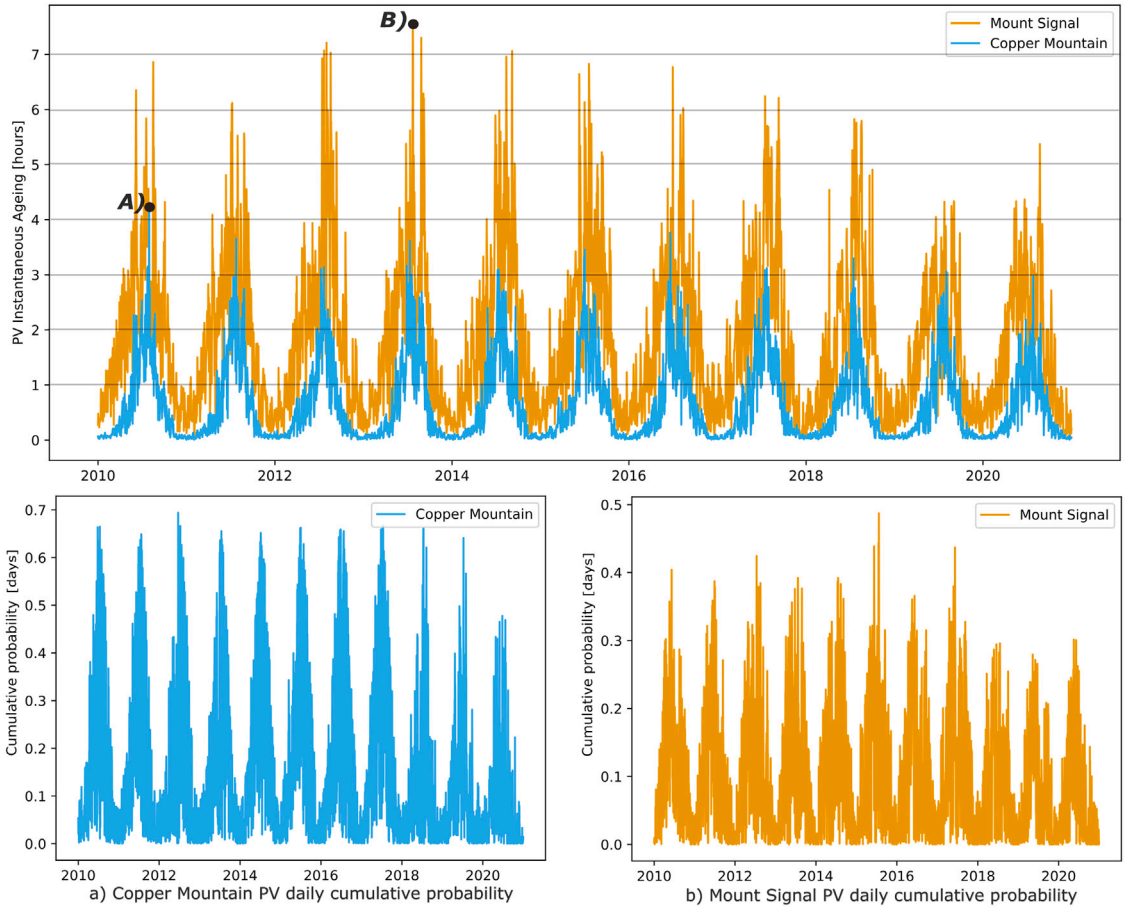

Fig. 12. Instantaneous hourly PV aging (top). Daily cumulative probability for PVs in (a) Copper Mountain and (b) Mount Signal (bottom).

The high degradation values observed in the PV modules of the Copper Mountain and Mount Signal II solar farms indicate the occurrence of significant degradation events at these facilities as shown in Fig. 12. These events can be caused by a variety of factors, such as extreme environmental conditions.

In the specific case of the Mount Signal II solar farm, the most significant PV instantaneous aging peak (7.52 h) occurred on July 23, 2013. At that time, the solar farm was exposed to extreme environmental conditions, with an irradiance of 972 W/m^2, a temperature of 41 °C, and a relative humidity of 69%. These conditions, reflected in the high degradation values recorded, may have contributed to the degradation of the PV modules.

It is important to note that this degradation event occurred in the context of the Aspen Fire, which began on 22 July 2013 and spread throughout southern California. The fire, which was caused by lightning, burned nearly 7300 acres and caused hazardous air quality in Mammoth Lakes and northern Inyo County [58]. The extreme weather conditions associated with the fire, such as high temperatures, low humidity, and intense solar radiation, likely contributed to the degradation of the PV modules.

Pollution from forest fires presents a considerable risk to photovoltaic (PV) systems in a number of ways. In particular, PM2.5 particles have the capacity to penetrate deeply into solar cells, thereby causing damage to the semiconductor materials therein. Furthermore,

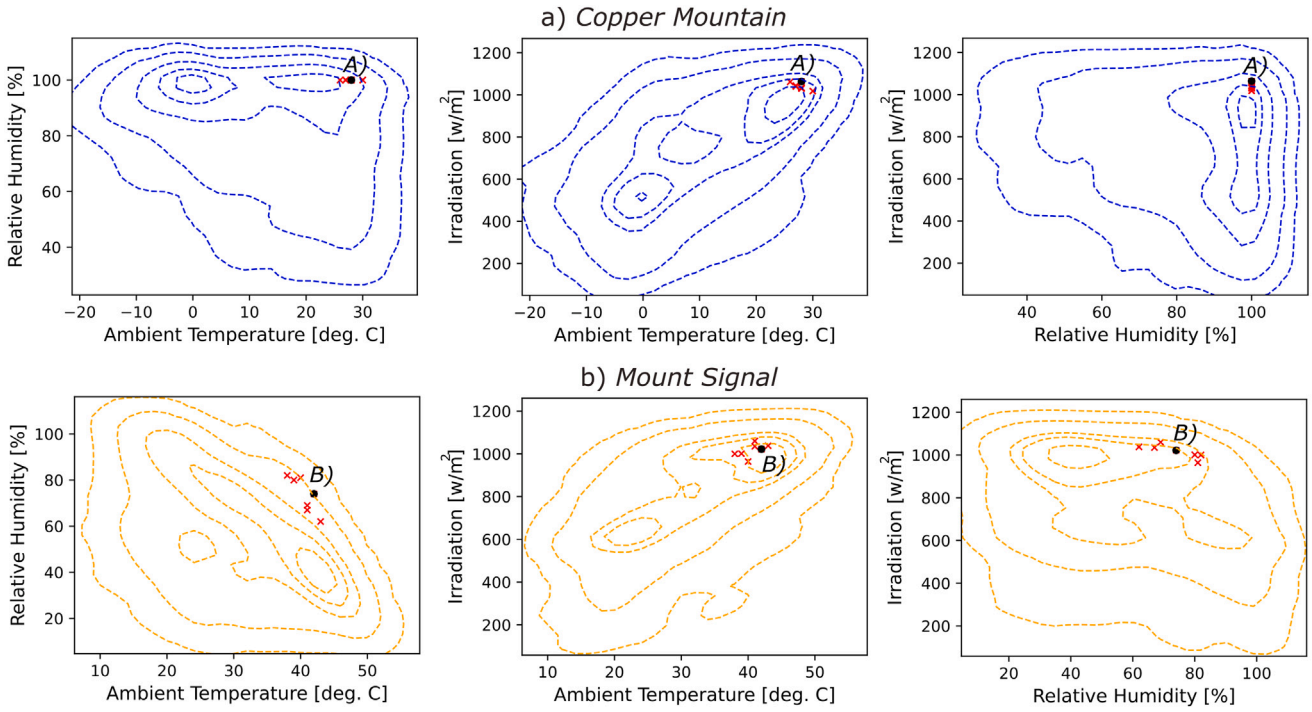

Fig. 13. Joint cumulative probability distribution hourly for PVs in (a) Copper Mountain and (b) Mount Signal.

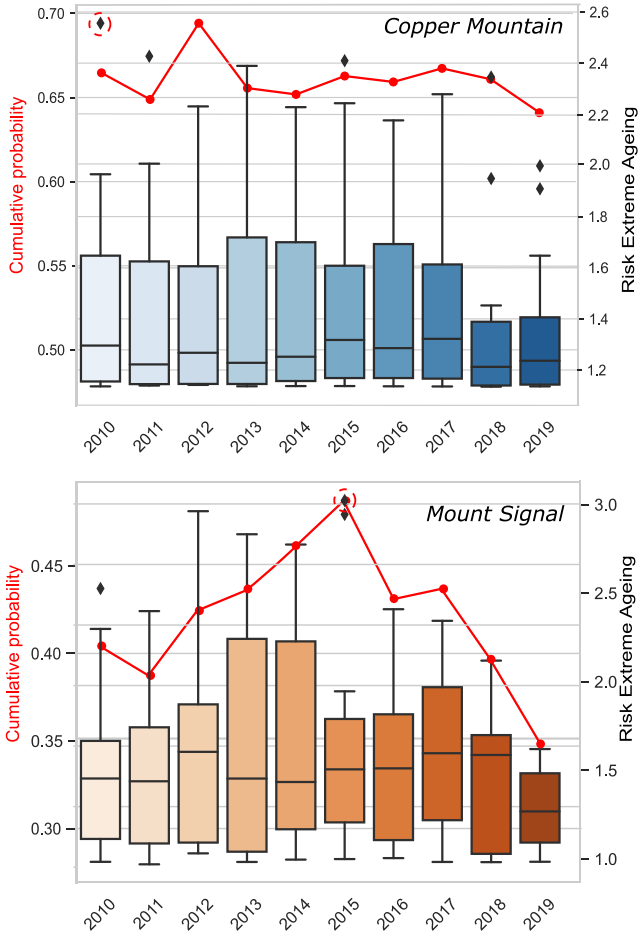

Fig. 14. Cumulative probability and PV panel risk index across the considered locations.

these particles diminish cell efficiency by scattering sunlight [59]. Contamination from forest fires represents a significant risk for PV systems, particularly in regions with elevated pollution levels or arid climates. In these environments, particulate matter can reduce solar power generation by over 50% if a suitable cleaning process is not employed, with the accumulation of dirt being the primary cause of this considerable decline in efficiency [60].

Furthermore, a significant risk of extreme aging peak occurred on 20 July 2015, as shown in Fig. 14. The corresponding extreme aging and degradation risk values were 3.02 and 6.83 h, respectively, accompanied by irradiance of 1001 W/m^2, ambient temperature of 39 °C, and relative humidity of 80%. This high risk of extreme aging also coincided with a period of intense wildfire activity in the western United States. In July, several large wildfires ravaged the region, including the Rocky Fire in Lake Country, California, and the Douglas Country Complex Fire in Washington [61]. It is likely that these wildfires, fueled by extreme weather conditions, caused this peak in risk.

Fig. 14 shows that the highest values of risk (2.56) and degradation (4.15 h) for Copper Mountain occurred on 2010-07-31. The irradiance was 991 W/m^2, the temperature was 29 °C, and the relative humidity was 100%. This may be likely caused by the wildfires in southern California at the time [62].

In this case, the maximum values of instantaneous aging in Fig. 12 are in agreement with the PV risk index in Fig. 14 (highlighted in red), which confirms a strong relationship between instantaneous aging, the risk index, and the extreme event phenomena developed in the temporal space analyzed.

Classification and analysis

Risk was also categorized based on the 25th, 75th, and 90th percentiles. Table 3 shows the risk levels for Copper Mountain and Mount Signal, based on their daily risk values.

The data indicate that both farms exhibit an identical distribution of days across all risk levels. However, Mount Signal consistently exhibits higher maximum risk values in each category, particularly in the critical risk level, where the risk reaches 3.03 compared to Copper Mountain's 2.56. This suggests that, although the temporal distribution of risk is comparable, Mount Signal is subjected to more extreme circumstances.

Table 3
Risk level classification for solar farms [days].

Farm	Risk level	Min	Max	Count
Copper Mountain	Low	9.30×10^{-9}	0.002370	1004
	Moderate	0.002370	0.158129	2007
	High	0.158383	0.563579	602
	Critical	0.566067	2.556143	402
Mount Signal	Low	2.11×10^{-10}	0.010263	1004
	Moderate	0.010277	0.349372	2007
	High	0.349436	0.720669	602
	Critical	0.723610	3.028415	402

5. Discussion

This research presents a risk assessment framework for power components operated in renewable energy power plants. The results show that the proposed approach captures extreme events and their consequences. However, before drawing definitive conclusions about the validity of the work, further work is necessary to test the approach for different extreme value considerations and timescales.

Risk sensitivity: extreme value & timescale

To test the sensitivity of the model with respect to the (i) timescale and (ii) extreme value, two different sensitivity assessments have been performed. On the one hand, a comprehensive multiscale temporal sampling strategy has been applied for wind energy (wind speed, temperature) and solar farm variables (solar irradiance, temperature, relative humidity) focused on daily, weekly, and monthly time intervals.

On the other hand, three specific percentiles have been used as extreme values including, the 75th, 95th and 100th (maximum) percentiles of the environmental variables at each timescale. The percentiles were calculated separately for each environmental variable. Evaluating the model's response to extreme events defined by each percentile allows for an assessment of its adaptability to varying degrees of extremity.

The results of this evaluation are presented in Tables 4 and 5, where the mean and maximum values of the hourly degradation risk index values under extreme conditions, *i.e.*, hours of loss-of-life in one hour are presented according to the different time scales and percentiles.

Table 4
Summary of WTT risk index (worst case highlighted).

Farm	Scale	Extreme Value					
		Mean			Maximum		
		100th	95th	75th	100th	95th	75th
Greece	day	0.041	0.042	0.048	2.49	2.52	2.67
Greece	week	0.023	0.027	0.049	1.98	2.17	2.76
Greece	month	0.013	0.018	0.052	1.65	2.12	2.81
USA	day	0.039	0.042	0.054	7.89	8.01	8.22
USA	week	0.013	0.028	0.055	6.29	7.95	8.28
USA	month	0.003	0.024	0.056	3.62	8.15	8.29
Vietnam	day	0.004	0.005	0.006	1.77	1.80	1.93
Vietnam	week	0.002	0.003	0.007	1.45	1.65	1.94
Vietnam	month	0.001	0.002	0.006	1.11	1.55	1.98

Table 5
Summary of solar panel risk index (worst case highlighted).

Farm	Scale	Extreme Value					
		Mean			Maximum		
		100th	95th	75th	100th	95th	75th
Copper	day	0.168	0.215	0.345	2.556	3.045	3.859
Copper	week	0.076	0.158	0.359	1.570	2.723	3.982
Copper	month	0.111	0.137	0.365	2.573	2.671	4.064
Mount	day	0.248	0.295	0.635	3.028	3.350	5.348
Mount	week	0.024	0.100	0.652	1.047	2.385	5.785
Mount	month	0.001	0.055	0.626	0.312	1.986	6.017

The results show a significant increase in risk index at the 75th percentile compared to the 100th and 95th percentiles. That is, the lower the quantile value, the higher the occurrence likelihood, but the lower the magnitude of the considered extreme value. This indicates an increased vulnerability with the highest probability of occurrence. Regarding the timescale, the results obtained show that the risk of extreme degradation significantly increases when evaluated on a daily timescale, compared to the risk estimated on the monthly and weekly scales.

At the 100th percentile, the highest mean value is observed on the daily scale and the maximum value of the series is recorded in the daily analysis. This pattern is repeated at the 95th percentile, except for the values related to the USA, where the maximum of the series corresponds to the monthly sample. On the other hand, at the 75th percentile, the highest risk index occurs in the monthly sample.

Weather conditions can exhibit much greater variability on a daily timescale than on a monthly or weekly timescale. This is due to the fluctuating nature of the daily weather conditions.

In the context of the 100th percentile, which represents the most extreme weather conditions, a significant increase in the risk index is detected on a daily scale. This is explained by the fact that extreme weather conditions, such as high winds or extreme temperatures, can cause significant damage to transformers and PV panels.

For the 95th percentile, which reflects adverse weather conditions, the risk index is also higher on a daily scale. However, the difference is not as pronounced as at the 100th percentile. This is because adverse conditions such as moderate winds, high temperatures, and high solar irradiation can cause damage to panels and transformers, although not necessarily to a significant extent.

The increasing frequency and intensity of extreme events, exacerbated by climate change, pose a significant threat to the energy infrastructure. Energy meteorologists make use of risk assessment frameworks to quantify the occurrence of extreme events and their impact. Accordingly, risk assessment methods generate valuable information to enable proactive measures to mitigate the impact of extreme weather events on energy systems. These frameworks consider factors such as the likelihood of extreme events, their potential severity, and the vulnerability of energy infrastructure to mitigate potential disruptions and ensure the reliable delivery of energy [3,63].

Influence of datasets

Moreover, it is important to note that while ERA5 is excellent at capturing large-scale atmospheric trends, it may underestimate the intensity of isolated events such as convection-driven thunderstorms. This could lead to a slight underestimation of events where high winds coincide with high temperatures.

Forecasting future risk

Gaussian copulas offer a robust framework for modeling dependencies in renewable energy systems under extreme weather events, as evidenced by studies analyzing cold and weak-wind events [8]. Their capacity to capture non-linear dependencies can be coupled with forecasting methodologies for a more accurate forecasting, e.g. integration of long short-term memory networks (LSTM) with copulas to predict system behaviors under extreme conditions [64], or Transformer models with copulas for time series forecasting [65]. The integration of Gaussian copulas with advanced ML techniques can enhance the accuracy and relevance of risk assessments, thereby facilitating more informed decision-making regarding the design, operation, and maintenance of renewable energy infrastructure. Furthermore, the integration of copula-based multivariate dependency models with machine learning (ML) and time-series forecasting has been shown to enhance both predictive accuracy and adaptability. A significant advantage of Gaussian copulas is their capacity to accommodate new data with ease.

As additional meteorological data becomes available, the copula model can be recalibrated to reflect updated dependencies and risk profiles. This iterative process guarantees that the model remains accurate and pertinent, which is of paramount importance for forecasting future risks under varying climate conditions. Techniques such as Bayesian updating or ML-based retraining can facilitate the seamless integration of new data, enabling continuous refinement and ensuring that decision-making is based on the most current information [66].

6. Conclusion

This study presents a probabilistic risk assessment framework to assess the impact of extreme weather events on wind turbine transformers (WTT) and photovoltaic (PV) panels. The framework integrates meteorological variables, aging considerations, and a Gaussian copula to predict the probability of extreme events. This probability of occurrence is used to quantify the risk index, which serves as an indicator of accelerated aging caused by extreme weather events.

Through different case studies for WTTs and solar PV panels conducted across diverse geographical locations, the framework demonstrates its efficacy in evaluating the risk posed by extreme weather events on these critical components of renewable energy infrastructure. The findings underscore the impact of extreme weather events on component aging, particularly during periods characterized by elevated temperatures for WTTs, and high solar irradiation for PV panels.

However, it is crucial to acknowledge the evolving nature of extreme weather events due to climate change. The return period of previously rare events, such as 1-in-10 year heatwaves, is likely to become significantly shorter in the future. By applying this framework with future climate projections, we can gain valuable insights into how climate change will influence transformer lifetime and prioritize infrastructure upgrades or maintenance strategies accordingly.

The integration of the risk index effectively combines the probability of extreme events with their degradation consequences, offering a valuable tool for identifying vulnerable components and prioritizing maintenance interventions. This study not only enhances our understanding of the influence of extreme weather events on renewable energy infrastructure but also provides actionable insights for developing targeted operation and maintenance strategies to mitigate their adverse effects.

Wildfire smoke presents unique challenges that may not be fully captured by existing models. It can penetrate PV cells, causing direct damage to semiconductor materials, and reduce the efficiency of solar panels by scattering sunlight. These effects highlight the importance of considering real-world environmental factors, such as wildfire pollution, in evaluating the resilience of PV systems. Future research may focus on the development of comprehensive risk assessment frameworks that integrate additional factors, such as wildfire smoke, dust and other environmental stressors, to evaluate their impact on renewable energy infrastructure. This would entail adapting the existing framework to evaluate the impact of extreme weather events, including wildfires, temperature increases, and particulate matter (e.g., PM10, PM2.5), on the efficiency and energy generation of photovoltaic systems or the impact of high wind speeds or gusts on potential damage or shut-down of wind farms. The development of advanced models would enable the quantification of the influence of rising temperatures, wildfire-related factors (including smoke and particulate deposition), and the urban heat island effect on the performance of these renewable energy systems. The incorporation of these factors into a broader risk index would facilitate a more comprehensive evaluation of the long-term degradation of system components, while also addressing the simultaneous impacts on power output and electricity demand.

The proposed framework would facilitate the formulation of more resilient strategies for the assurance of renewable energy infrastructure. The resultant metrics could then be applied to climate change projections to understand how the increasing frequency and intensity of extreme weather events may cause challenges to future energy system resilience. Such strategies could also encompass predictive modeling to evaluate potential supply–demand imbalances under disparate extreme weather scenarios, thereby aiding the optimization of grid management in the context of both diminished energy production and augmented consumption during peak demand periods.

CRediT authorship contribution statement

Nadia N. Sánchez-Pozo: Writing – original draft, Visualization, Validation, Software, Methodology, Investigation. **Erik Vanem:** Writing – original draft, Validation, Supervision, Conceptualization. **Hannah Bloomfield:** Writing – original draft, Visualization, Validation. **Jose I. Aizpurua:** Writing – original draft, Supervision, Resources, Project administration, Methodology, Funding acquisition, Conceptualization.

Declaration of competing interest

The authors declare that they have no known competing financial interests or personal relationships that could have appeared to influence the work reported in this paper.

Acknowledgments

This research was funded by the Department of Education of the Basque Government (grant No. KK-2023-00041 and IT1504-22). In addition, J. I. Aizpurua is funded by the Ramón y Cajal Fellowship, Spanish State Research Agency (grant number RYC2022-037300-I), co-funded by MCIU/ AEI/ 10.13039/ 501100011033 and FSE+.

Appendix A. PV panel aging

The derivative of the PV aging factor in Eq. (19) was calculated to evaluate the effect of environmental factors such as daily maximum temperature Θ_{max} [K], daily average temperature $\Delta\Theta_{daily}$ [K], daily average irradiation UV_{daily} [W/m^2] and humidity RH_{daily} [%], on the aging of photovoltaic panels, as follows:

$$\frac{\partial F_{A_{PV}}}{\partial \Theta_{max}} = \frac{\beta_0\beta_1}{k_B\Theta_{max}^2} e^{\frac{-\beta_1}{k_B\Theta_{max}}} \Delta\Theta_{daily}^{\beta_2} UV_{daily}^{\beta_3} RH_{daily}^{\beta_4} \tag{21}$$

$$\frac{\partial F_{A_{PV}}}{\partial \Delta\Theta_{daily}} = \beta_2\beta_0\Delta\Theta_{daily}^{\beta_2-1} e^{\frac{-\beta_1}{k_B\Theta_{max}}} UV_{daily}^{\beta_3} RH_{daily}^{\beta_4} \tag{22}$$

The results of the analysis showed a direct correlation between the maximum temperature and the PV aging factor. This means that the degradation process of PV panels is accelerated at higher temperatures, as shown in the Fig. 15. This finding is consistent with previous studies that have attributed accelerated degradation to increased thermal stress and degradation of chemical bonds within the PV cells [67]. The analysis also considered the effect of temperature difference, defined as the difference between the maximum temperature and the ambient temperature. In addition, the results showed a positive correlation between the temperature difference and the PV aging factor, suggesting that larger temperature fluctuations may accelerate the degradation of PV panels. This could be explained by the expansion and contraction of PV materials due to temperature changes, resulting in mechanical stress and potential damage [68].

$$\frac{\partial F_{A_{PV}}}{\partial UV_{daily}} = \beta_3\beta_0\Delta\Theta_{daily}^{\beta_2} e^{\frac{-\beta_1}{k_B\Theta_{max}}} UV_{daily}^{\beta_3-1} RH_{daily}^{\beta_4} \tag{23}$$

$$\frac{\partial F_{A_{PV}}}{\partial RH_{daily}} = \beta_4\beta_0 e^{\frac{-\beta_1}{k_B\Theta_{max}}} \Delta\Theta_{daily}^{\beta_2} UV_{daily}^{\beta_3} RH_{daily}^{\beta_4-1} \tag{24}$$

A positive correlation is observed between relative humidity and the photovoltaic aging factor, high humidity levels can negatively impact the efficiency and longevity of solar panels by promoting dust accumulation, corrosion, moisture damage, and contributing to potential-induced degradation, highlighting the importance of considering humidity as a significant factor in the degradation of PV panels [69].

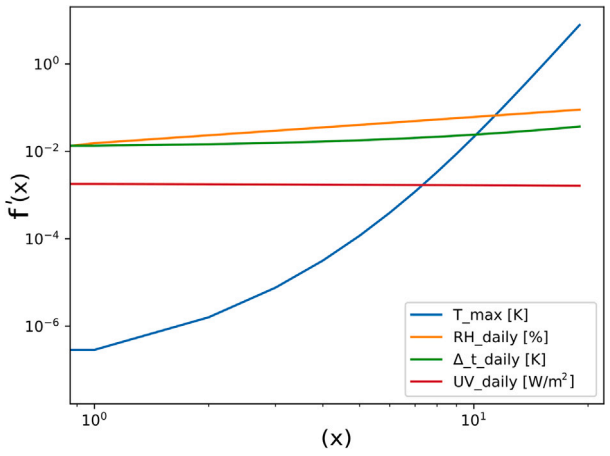

Fig. 15. PV aging factor rate-of-change with respect to different factors.

References

[1]E. Laino, G. Iglesias, Extreme climate change hazards and impacts on European coastal cities: A review, Renew. Sustain. Energy Rev. 184 (2023) 113587, http://dx.doi.org/10.1016/j.rser.2023.113587.

[2]E. Rousi, K. Kornhuber, G. Beobide-Arsuaga, F. Luo, D. Coumou, Accelerated western European heatwave trends linked to more-persistent double jets over Eurasia, Nat. Commun. 13 (1) (2022) 3851.

[3]B. Clarke, F. Otto, R. Stuart-Smith, L. Harrington, Extreme weather impacts of climate change: an attribution perspective, Environ. Res. Clim. 1 (1) (2022) 012001.

[4]J. Beyza, J.M. Yusta, The effects of the high penetration of renewable energies on the reliability and vulnerability of interconnected electric power systems, Reliab. Eng. Syst. Saf. 215 (2021) 107881, http://dx.doi.org/10.1016/j.ress.2021.107881.

[5]L. Xu, K. Feng, N. Lin, A. Perera, H.V. Poor, L. Xie, C. Ji, X.A. Sun, Q. Guo, M. O'Malley, Resilience of renewable power systems under climate risks, Nat. Rev. Electr. Eng. 1 (1) (2024) 53–66.

[6]T. Reindl, W. Walsh, Z. Yanqin, M. Bieri, Energy meteorology for accurate forecasting of PV power output on different time horizons, Energy Procedia 130 (2017) 130–138.

[7]L. Rapella, D. Faranda, M. Gaetani, P. Drobinski, M. Ginesta, Climate change on extreme winds already affects off-shore wind power availability in Europe, Environ. Res. Lett. 18 (2023) http://dx.doi.org/10.1088/1748-9326/acbdb2.

[8]P. Tedesco, A. Lenkoski, H.C. Bloomfield, J. Sillmann, Gaussian copula modeling of extreme cold and weak-wind events over Europe conditioned on winter weather regimes, Environ. Res. Lett. 18 (3) (2023) 034008, http://dx.doi.org/10.1088/1748-9326/acb6aa.

[9]B. H.C., H. J., G. A., K. A.L., S. L.C., P. F., J. R., K. D., C. A., B. P.D., Co-occurring wintertime flooding and extreme wind over Europe, from daily to seasonal timescales, Weather Clim. Extrem. 39 (2023) 100550, http://dx.doi.org/10.1016/j.wace.2023.100550, URL https://www.sciencedirect.com/science/article/pii/S2212094723000038.

[10]N.A. Ibrahim, S.R. Wan Alwi, Z.A. Manan, A.A. Mustaffa, K. Kidam, Risk matrix approach of extreme temperature and precipitation for renewable energy systems in Malaysia, Energy 254 (2022) 124471, http://dx.doi.org/10.1016/j.energy.2022.124471.

[11]E. Vanem, 3-dimensional environmental contours based on a direct sampling method for structural reliability analysis of ships and offshore structures, Ships Offshore Struct. 14 (1) (2019) 74–85, http://dx.doi.org/10.1080/17445302.2018.1478377.

[12]E. Ross, O.C. Astrup, E. Bitner-Gregersen, N. Bunn, G. Feld, B. Gouldby, A. Huseby, Y. Liu, D. Randell, E. Vanem, P. Jonathan, On environmental contours for marine and coastal design, Ocean Eng. 195 (2020) 106194, http://dx.doi.org/10.1016/j.oceaneng.2019.106194, URL https://www.sciencedirect.com/science/article/pii/S0029801819303798.

[13]G. Miloshevich, B. Cozian, P. Abry, P. Borgnat, F. Bouchet, Probabilistic forecasts of extreme heatwaves using convolutional neural networks in a regime of lack of data, Phys. Rev. Fluids 8 (2023) 040501, http://dx.doi.org/10.1103/PhysRevFluids.8.040501.

[14]M. Penalba, J.I. Aizpurua, A. Martinez-Perurena, On the definition of a risk index based on long-term metocean data to assist in the design of Marine Renewable Energy systems, Ocean Eng. 242 (2021) 110080, http://dx.doi.org/10.1016/j.oceaneng.2021.110080.

[15]E. Vanem, Uncertainties in extreme value modelling of wave data in a climate change perspective, J. Ocean Eng. Mar. Energy 1 (2015) 339–359.

[16]E. Vanem, Analysing multivariate extreme conditions using environmental contours and accounting for serial dependence, Renew. Energy 202 (2023) 470–482, http://dx.doi.org/10.1016/j.renene.2022.11.033.

[17]A. Perera, V.M. Nik, D. Chen, J.-L. Scartezzini, T. Hong, Quantifying the impacts of climate change and extreme climate events on energy systems, Nat. Energy 5 (2) (2020) 150–159.

[18]I. Staffell, R. Green, How does wind farm performance decline with age? Renew. Energy 66 (2014) 775–786.

[19]S.R. Khuntia, J.L. Rueda, M.A. van der Meijden, Risk-based security assessment of transmission line overloading considering spatio-temporal dependence of load and wind power using vine copula, IET Renew. Power Gener. 13 (10) (2019) 1770–1779.

[20]R. Wei, S. Hu, F. Yang, G. Shi, D. Zhang, L. Zhang, X. Fang, X. Tan, J. Huang, New energy power prediction and warning based on multi-source prediction and scene classification recognition, Procedia Comput. Sci. 224 (2023) 401–406.

[21]Q. Chen, X. Xiong, C. Xiao, L. He, Y. Pu, H. Chen, The probabilistic assessment of outgoing transformer operation risk considering the correlation between wind power and photovoltaic, in: 2019 IEEE Sustainable Power and Energy Conference, ISPEC, 2019, pp. 1785–1790, http://dx.doi.org/10.1109/iSPEC48194.2019.8975137.

[22]J. Zhou, C. He, Risk assessment of power system under extreme typhoon events, in: 2023 5th Asia Energy and Electrical Engineering Symposium, AEEES, IEEE, 2023, pp. 724–728.

[23]E. Chiodo, B. Diban, G. Mazzanti, F. De Angelis, A review on wind speed extreme values modeling and estimation for wind power plant design and construction, Energies 16 (14) (2023).

[24]N.J. Cook, Reliability of extreme wind speeds predicted by extreme-value analysis, Meteorology 2 (3) (2023) 344–367, http://dx.doi.org/10.3390/meteorology2030021.

[25]G.K. Sakki, I. Tsoukalas, P. Kossieris, C. Makropoulos, A. Efstratiadis, Stochastic simulation-optimization framework for the design and assessment of renewable energy systems under uncertainty, Renew. Sustain. Energy Rev. 168 (2022) 112886.

[26]X. Lin, J. Fang, H. Wang, C. Gu, K. Yin, M. Zhang, F. Mo, Probabilistic assessment of transformer operating risk considering the correlation among wind power, PV and load, in: International Conference on Mechanical Engineering, Measurement Control, and Instrumentation, Vol. 11930, SPIE, 2021, pp. 30–38.

[27]O.A. Ansari, Y. Gong, W. Liu, C.Y. Chung, Data-driven operation risk assessment of wind-integrated power systems via mixture models and importance sampling, J. Mod. Power Syst. Clean Energy 8 (3) (2020) 437–445.

[28]N.G. Leveson, Engineering a Safer World: Systems Thinking Applied to Safety, The MIT Press, 2012, http://dx.doi.org/10.7551/mitpress/8179.001.0001.

[29]N. Wang, Y. Du, D. Chen, H. Meng, X. Chen, L. Zhou, G. Shi, Y. Zhan, M. Feng, W. Li, et al., Spatial disparities of ozone pollution in the sichuan basin spurred by extreme, hot weather, Atmos. Chem. Phys. 24 (5) (2024) 3029–3042.

[30]Copula modeling: An introduction for practitioners, Found. Trends Econom. 1 (1) (2005) 1–111, http://dx.doi.org/10.1561/0800000005.

[31]E. Vanem, Joint statistical models for significant wave height and wave period in a changing climate, Mar. Struct. 49 (2016) 180–205, http://dx.doi.org/10.1016/j.marstruc.2016.06.001, URL https://www.sciencedirect.com/science/article/pii/S095183391630106X.

[32]N. Otero, O. Martius, S. Allen, H. Bloomfield, B. Schaefli, A copula-based assessment of renewable energy droughts across europe, Renew. Energy 201 (2022) 667–677, http://dx.doi.org/10.1016/j.renene.2022.10.091.

[33]M.R. Hussain, S. Refaat, H. Abu-Rub, Overview and partial discharge analysis of power transformers: A literature review, IEEE Access 9 (2021) 64587–64605, http://dx.doi.org/10.1109/ACCESS.2021.3075288.

[34]O. Segbefia, T. Sætre, Investigation of the temperature sensitivity of 20-years old field-aged photovoltaic panels affected by potential induced degradation, Energies (2022) http://dx.doi.org/10.3390/en15113865.

[35]T. Rahman, A.A. Mansur, M.S.H. Lipu, M. Rahman, R.H. Ashique, M.A. Houran, R. Elavarasan, E. Hossain, Investigation of degradation of solar photovoltaics: A review of aging factors, impacts, and future directions toward sustainable energy management, Energies (2023) http://dx.doi.org/10.3390/en16093706.

[36]H. Hersbach, B. Bell, P. Berrisford, S. Hirahara, A. Horányi, J. Muñoz-Sabater, J. Nicolas, C. Peubey, R. Radu, D. Schepers, et al., The ERA5 global reanalysis, Q. J. R. Meteorol. Soc. 146 (730) (2020) 1999–2049.

[37]S. Haas, B. Schachler, U. Krien, S. Bosch, Windpowerlib: a Python Library to Model Wind Power Plants (V0.1.0), Zenodo, 2019, http://dx.doi.org/10.5281/zenodo.2542896.

[38]J.I. Aizpurua, I. Ramirez, I. Lasa, L.d. Rio, A. Ortiz, B.G. Stewart, Hybrid transformer prognostics framework for enhanced probabilistic predictions in renewable energy applications, IEEE Trans. Power Deliv. 38 (1) (2023) 599–609, http://dx.doi.org/10.1109/TPWRD.2022.3203873.

[39]J.I. Aizpurua, R. Peña-Alzola, J. Olano, I. Ramirez, I. Lasa, L. del Rio, T. Dragicevic, Probabilistic machine learning aided transformer lifetime prediction framework for wind energy systems, Int. J. Electr. Power Energy Syst. 153 (2023) 109352, http://dx.doi.org/10.1016/j.ijepes.2023.109352.

[40]IEC, Loading guide for oil-immersed power transformers, 2018, IEC 60076-7.
[41]M. Sengupta, Y. Xie, A. Lopez, A. Habte, G. Maclaurin, J. Shelby, The National Solar Radiation Data Base (NSRDB), Renew. Sustain. Energy Rev. 89 (2018) 51–60, http://dx.doi.org/10.1016/j.rser.2018.03.003.
[42]D.L. King, W.E. Boyson, J.A. Kratochvil, Photovoltaic Array Performance Model, Vol. 8, Sandia Report No. 2004-3535, 2004, pp. 1–19, http://dx.doi.org/10.2172/919131, URL http://www.osti.gov/bridge/product.biblio.jsp?osti_id=919131.
[43]I. Kaaya, J. Ascencio-Vásquez, K.-A. Weiss, M. Topič, Assessment of uncertainties and variations in PV modules degradation rates and lifetime predictions using physical models, Sol. Energy 218 (2021) 354–367, http://dx.doi.org/10.1016/j.solener.2021.01.071.
[44]I. Kaaya, M. Koehl, A.P. Mehilli, S. de Cardona Mariano, K.A. Weiss, Modeling outdoor service lifetime prediction of PV modules: effects of combined climatic stressors on PV module power degradation, IEEE J. Photovolt. 9 (4) (2019) 1105–1112.
[45]A.B. Subramaniyan, R. Pan, J. Kuitche, G. TamizhMani, Quantification of environmental effects on PV module degradation: A physics-based data-driven modeling method, IEEE J. Photovolt. 8 (5) (2018) 1289–1296.
[46]IEA, Service Life Estimation 4 PV Modules, Tech. Rep., IEA, Paris, France, 2021.
[47]A. Bala Subramaniyan, R. Pan, J. Kuitche, G. TamizhMani, Quantification of environmental effects on PV module degradation: A physics-based data-driven modeling method, IEEE J. Photovolt. 8 (5) (2018) 1289–1296, http://dx.doi.org/10.1109/JPHOTOV.2018.2850527.
[48]PyPI Contributors, copulas: A Python library for copulas and multivariate dependence modeling, 2020, URL https://pypi.org/project/copulas/. (Accessed 18 November 2024).
[49]SciPy Developers, SciPy: Open source scientific tools for Python, 2024, URL https://scipy.org/. (Accessed 18 November 2024).
[50]Scikit-learn Developers, scikit-learn: Machine Learning in Python, 2024, URL https://scikit-learn.org/. (Accessed 18 November 2024).
[51]Matplotlib Development Team, Matplotlib: A comprehensive library for creating static, animated, and interactive visualizations in Python, 2024, URL https://matplotlib.org/. (Accessed 18 November 2024).
[52]SciPy Developers, scipy.stats.anderson_ksamp - SciPy Documentation, 2024, URL https://docs.scipy.org/doc/scipy/reference/generated/scipy.stats.anderson_ksamp.html. (Accessed 22 November 2024).
[53]R.H. Grumm, The central European and Russian heat event of july–august 2010, Bull. Am. Meteorol. Soc. 92 (2011) 1285–1296, http://dx.doi.org/10.1175/2011BAMS3174.1.
[54]NOAA National Centers for Environmental Information, Monthly national climate report for june 2011, 2011, URL https://www.ncei.noaa.gov/access/monitoring/monthly-report/national/201106. Published online July 2011.
[55]D. Khang, Hanoi residents grapple with fresh heat wave, 2018, Tuoi Tre News URL https://tuoitrenews.vn/news/society/20180702/hanoi-residents-grapple-with-fresh-heat-wave/46486.html.
[56]N. Politi, D. Vlachogiannis, A. Sfetsos, P.T. Nastos, High resolution projections for extreme temperatures and precipitation over Greece, Clim. Dyn. 61 (1–2) (2023) 633–667.
[57]L.H. Ba, T.V. Nam, L. Hung, Collection & investigation on flash flood characteristics (case study: Dak Lak Province), in: Flash Floods in Vietnam: Causes, Impacts, and Solutions, Springer International Publishing, Cham, 2022, pp. 35–65, http://dx.doi.org/10.1007/978-3-031-10532-6_3.
[58]NOAA National Centers for Environmental Information, Monthly National Climate Report for July 2013, 2013, URL https://www.ncei.noaa.gov/access/monitoring/monthly-report/national/201307. (Published online August 2013, retrieved on December 1, 2023).
[59]S.D. Gilletly, N.D. Jackson, A. Staid, Evaluating the impact of wildfire smoke on solar photovoltaic production, Appl. Energy 348 (2023) 121303.
[60]X. Li, D. Mauzerall, M. Bergin, Global reduction of solar power generation efficiency due to aerosols and panel soiling, Nat. Sustain. (2020) 1–8, http://dx.doi.org/10.1038/s41893-020-0553-2.
[61]NOAA National Centers for Environmental Information, Monthly national climate report for july 2015, 2015, URL https://www.ncei.noaa.gov/access/monitoring/monthly-report/national/201507. (Retrieved on December 1, 2023) Published online.
[62]NOAA National Centers for Environmental Information, Monthly wildfires report for july 2010, 2010, URL https://www.ncei.noaa.gov/access/monitoring/monthly-report/fire/201007.
[63]A. Grochowicz, K. van Greevenbroek, H.C. Bloomfield, A new method for identifying weather-induced power system stress using shadow prices, 2023, arXiv:2307.13520.
[64]S. Han, Q. Yanhui, J. Yan, Y. Liu, L. Li, Z. Wang, Mid-to-long term wind and photovoltaic power generation prediction based on copula function and long short term memory network, Appl. Energy (2019) http://dx.doi.org/10.1016/J.APENERGY.2019.01.193.
[65]A. Drouin, É. Marcotte, N. Chapados, Tactis: Transformer-attentional copulas for time series, in: International Conference on Machine Learning, PMLR, 2022, pp. 5447–5493.
[66]N. Mararakanye, A. Dalton, B. Bekker, Characterizing wind power forecast error using extreme value theory and copulas, IEEE Access PP (2022) 1, http://dx.doi.org/10.1109/access.2022.3179697.
[67]M. Aghaei, A. Fairbrother, A. Gok, S. Ahmad, S. Kazim, K. Lobato, G. Oreski, A. Reinders, J. Schmitz, M. Theelen, P. Yilmaz, J. Kettle, Review of degradation and failure phenomena in photovoltaic modules, Renew. Sustain. Energy Rev. 159 (2022) 112160, http://dx.doi.org/10.1016/j.rser.2022.112160, URL https://linkinghub.elsevier.com/retrieve/pii/S1364032122000880.
[68]K. Khanafer, A. Al-Masri, A. Marafie, K. Vafai, Thermal performance of solar photovoltaic panel in hot climatic regions: Applicability and optimization analysis of PCM materials, Numer. Heat Transfer A (2023) 1–21, http://dx.doi.org/10.1080/10407782.2023.2207732, URL https://www.tandfonline.com/doi/full/10.1080/10407782.2023.2207732.
[69]A.K. Tripathi, S. Ray, M. Aruna, S. Prasad, Evaluation of solar PV panel performance under humid atmosphere, Mater. Today Proc. 45 (2021) 5916–5920, http://dx.doi.org/10.1016/j.matpr.2020.08.775, URL https://linkinghub.elsevier.com/retrieve/pii/S2214785320366591.